(2)

MICROSTRUCTURAL DEVELOPMENT IN HSLA-100 STEEL WELD METALS

Final Report
Grant No. N00014-89-J-1958

Submitted by

Paul R. Howell
Professor of Metals Science and Engineering
The Pennsylvania State University
University Park, PA 16802

Overview

In light of the fact that much of the last year's research effort is in press, or will be submitted for publication shortly, this second year report consists primarily of these manuscripts. This overview presents the issues which are contained in the research papers, and also indicates regions of research which have been examined but are not contained herein. These latter areas will be written for publication and submitted as Appendices to this report. It is envisaged that all publications will be completed before the end of summer. At this point it should be noted that there is very little overlap between the content of this second year report are that which was presented in the first year's progress report.

In order to check the validity of the data from the as-received plate (see last year's report), samples were re-austenitized, quenched and subsequently tempered for up to 3 hours at 605°C. The results of this investigation are given in pages 1-8 and figures are presented on pages 11-15.

In order to document the long term, high temperature stability of HSLA-100, tempering times were increased up to 48 hours. Results are given on pages 22-23 and figures are presented on pages 30-32.

The microstructures that develop in the coarse-grained heat affected zone (CG-HAZ) of the welds are discussed on page 21 and figures are found on p. 29. At this point, it should be noted that all of the results reported herein are for the 0.04%C version of HSLA-100. We have also examined an 0.02%C version, and the results of these studies (primarily with respect to quenching/tempering and the CG-HAZ) will be submitted shortly.

The effects of air-cooling from the austenite range (approximately $7°s^{-1}$ cooling rate) have been documented (see pages 23 and 65 for a discussion and pages 38-39 and 66 for figures). A more complete discussion of the effects of air-cooling is being written, in

conjunction with the results of the furnace cooling study (see last year's report).

On the basis of some of the microstructural data from last year, a tentative proposal for the formation of "Granular Bainite" was advanced. In order to verify this proposal, a steel of the same carbon level (0.04%C), but also with a low substitutional content was re-examined. The results of this re-examination are presented in pages 40-51 with figures on pages 52-64.

Finally, a brief introduction to the isothermal studies is presented on page 65 and figures are given on page 66. Again, a more detailed account of these important studies is presently being written.

To be published in : " *Microstructural Science* "
ed. G.S. Cole. International Metallographic Society, Columbus, OH

THE APPLICATION OF METALLOGRAPHIC TECHNIQUES TO THE STUDY OF TEMPERING IN ULTRA-LOW CARBON STEELS

R. Varughese and P. R. Howell*

ABSTRACT

This paper is concerned with a study of a quenched and quenched and tempered low carbon, copper containing steel (HSLA 100). The primary investigative technique employed has been transmission electron microscopy (TEM). Quenching the steel from the austenitizing temperature yields a microstructure which is predominantly lath martensite. However, a significant amount of retained austenite is also present. Niobium carbide particles have also been documented in the as-quenched structures.

Tempering at 605°C for one to three hours yields a heterogeneous distribution of ε-Cu, much of which is associated with the lath boundaries. The austenite is highly resistant to decomposition during tempering at 605°C and as a consequence, little evidence for cementite precipitation has been found.

INTRODUCTION

Precipitation strengthening of steel by finely dispersed copper particles has played a key role in the development of the low carbon HSLA series of steels possessing very high strength, toughness, and superior weldability. HSLA-100 alloy, intended to meet a minimum yield strength of 100 ksi through a quench and temper heat treatment procedure, combines the austenite grain refining influence of niobium and the hardenability contribution from Mn, Ni, Cr and Mo to achieve a fine lath microstructure through commercial water quenching means. The quenched material is subsequently aged to provide a uniform distribution of copper precipitates while

* Department of Materials Science and Engineering. The Pennsylvania State University, University Park, PA 16802.

allowing for some recovery of the as-quenched microstructure. The resulting fine ferritic grain size is the principal factor contributing to the high strength-toughness combination for the HSLA-100 steel. The new steel, with its low carbon content, would permit less stringent welding procedures as well as reduce the mechanical property deterioration from welding operations.

The development of the ultra low carbon HSLA-100 steel has been aided by the somewhat detailed data base on the structure-property interrelationships and weldability characteristics on the copper strengthened ferrite-pearlite steel commonly referred to as ASTM A710 [1-4], which is also known as HSLA-80 despite the higher alloying content as compared to the microalloyed HSLA steels. Since the acceptance of HSLA-80 as an alternative to the carbon-rich HY-80 for several marine construction applications, the U.S. Navy has supported a vigorous program in developing tougher grades to meet strength levels in excess of 100 ksi while reducing the carbon levels to the 0.02-0.04 wt% range to ensure good weldability [5,6]. The alloy chemistry chosen for the HSLA-100 has therefore, been considerably richer in nickel and copper as compared to the HSLA-80. This chemistry modification is aimed at maximizing the hardenability effects and thereby producing a fully martensite/bainite morphology if not a fully martensitic microstructure in thick sections through quenching from the solution treatment temperature [7]. Furthermore, it has been reported that at this reduced level, carbon contribution to hardenability is very pronounced and that the HSLA-100 with 0.04 wt% carbon tended to produce a martensite/bainite mixture as compared to a fully martensitic microstructure in the same alloy with 0.06 wt% carbon [8]. However, detailed microstructural studies of HSLA-100 steel have not been reported so far.

The present study therefore, addresses the basic microstructural development in samples quenched from the solution-treatment temperature and the influence of this microstructure on the precipitation of ε-copper during the aging heat treatment and the precipitation of other carbides such as cementite in the microstructure.

EXPERIMENTAL APPROACH

Material for the study was taken from a 31mm thick plate from Lukens Steel Co. The chemical composition of the alloy in given in Table 1. The as-received plate was solution treated at 905°C for 75 minutes and water quenched followed by the aging heat treatment at 640°C for 75 minutes and subsequently water quenched. Samples for this work were reaustenitized at 1000°C for 10 minutes and were then oil or water quenched. Oil quenched specimens were aged for 1 hour and 3 hours at 605°C and air-cooled.

Specimens for optical microscopy were prepared using standard metallographic techniques and were etched in a mixture of 4% picral-1% nital. Thin foil TEM specimens were prepared in a twin-jet electropolisher using an electrolyte containing 5% perchloric acid (by volume) in glacial acetic acid at room temperature and at a potential of 40-50 volts. TEM was performed on a Philips EM420T operating at 120 kV.

RESULTS

Microstructure of the Quenched Material

The as-quenched microstructure of the HSLA-100 is lath martensite as seen from the optical micrograph presented in Figure 1. Though the prior austenite grain boundaries are not clearly evident , the transformed microstructure can be described as equiaxed packets of thin laths with a common orientation within each packet. The oil-quenching material had a microhardness of VHN 310-325 which is only slightly lower than the VHN 320-330 found in water quenched material.

Figure 2 shows the typical lath martensitic microstructure of the as quenched steel. The bright field (BF) TEM micrograph in Figure 2 reveals the narrow, elongated laths within a packet. The median packet size is about 3-5 μm as are the long dimensions of the laths. The laths are approximately 0.2 to 0.3 μm in width and their microstructures are characterized by a heavily dislocated substructure. While the structure may be categorized as primarily fine lath martensite,

large martensitic grains have been observed occasionally, a few of which have been noted to contain fine twins.

The principal second phase constituent identified in the quenched steel was retained austenite, present as either films or as larger particles at the interlath boundaries as seen from the centered dark field (CDF) image of Figure 3. The elongated austenitic constituents at the interlath boundaries are about 0.05 to 0.1μm in width while the length dimensions range from 0.2 to a few μm.

Niobium carbide particles have been found to be present in the quenched materials in sizes ranging from 10 nm to about 25 nm and are observed both along the lath boundaries as well as in the ferritic matrix. A typical example of the distribution of niobium carbide is shown in the CDF image of Figure 4a. The associated selected area diffraction (SAD) pattern in Figure 4b is indexed in terms of the ferritic matrix, together with niobium carbide, the latter having a lattice parameter of 0.44 nm.

Microstructure of the Aged Material

In general, the microstructure of the aged material reveals regions of aligned lath constituents as well as regions with a more equiaxed morphology resembling that of granular bainite. Considering the as-quenched microstructure to be lath martensite, the aged material may be referred to as tempered martensite. Comparison of the basic morphology after aging at 605°C for 1 hr. and 3 hrs respectively indicated that the ferritic structure is fairly insensitive to these aging times. Microhardness measurements gave nearly identical VHN of about 275 for the two aged conditions as compared to the average VHN 320 for the quenched material. The reduced hardness is an indication of the softening of the microstructure resulting from recovery of the heavily dislocated lath microstructure as well as the (presumed) overaged condition of the precipitated copper in the alloy.

TEM examination of thin foils in the aged materials clearly reveals the microstructural changes that lead to the observed softening. Although a significant fraction of the as-quenched lath

structure is preserved as seen from the BF/CDF image pair shown in Figures 5a and b, tempering causes substantial recovery, resulting in the granular ferrite morphology apparent in optical micrographs. Reference to figure 5b also shows that many of the laths have a similar orientation.

The most important microstructural development during ageing of this alloy is the precipitation of ε-copper particles. Aging at 605°C for 1 hour is considered to leave the steel in the overaged condition [8] to ensure adequate fracture toughness while satisfying strength requirements. The 3-hour ageing study was carried out to assess the influence of coarsening on the copper precipitates.

After the 1 hour age, the alloy contains a non-uniform dispersion of ε-Cu precipitates as illustrated in the γ/ε CDF of Figure 6a. The ε -Cu particles exist in a wide size range about 6-20 nm. Whereas many of these particles may be considered spherical or nearly-spherical, the particles at the upper end of the size spectrum tended to be rod-shaped and were mostly associated with the lath boundaries. Another aspect of the ε-Cu precipitate distribution in Figure 6a is that most of the particles in this region are imaged with a single (002) ε -Cu reflection. This might indicate that one of the 24 possible orientation variants of the Kurdjumov-Sachs (K-S) is dominant. This variant is cube/cube related to the retained austenite as shown in the γ/ε CDF of Figure 6a and the indexed diffraction pattern of Figure 6b.

After three hours, the ε-Cu precipitates were much coarser (in the size range of 10 to 50 nm) as shown in the γ/ε CDF of Figure 7.

Reference to Figures 6 and 7 shows that the retained austenite found in the as-quenched material is little affected by the aging heat treatments and remains as the principal second phase constituent. Figure 8a is a BF micrograph of elongated intralath austenite whereas the CDF image in Figure 8b reveals irregular shaped particles associated with the granular ferritic morphology. Figure 8c is an indexed convergent beam electron diffraction (CBED) pattern from a small isolated austenite particle.

Other second phase particles were noted principally along the grain/lath boundaries. Many of these particles were about 50-100 nm in size and several such particles in the 3 hours aged

specimen have been found to be coarsened copper precipitates. However, in addition to the niobium carbide which was present in the quenched samples, cementite has been identified in the aged condition.

DISCUSSION

The results presented in Section 3 indicate that rapid quenching of the HSLA-100 alloy from the solution treatment temperature leads to a primarily lath martensitic microstructure with a high density of dislocations. Therefore, the lower microhardness values $\simeq$ VH320 as compared with that noted by Wilson et al [8] in the 0.06% C HSLA-100 alloy is the result of the reduced hardenability, or equivalently a higher martensitic start temperature.

The dominant second phase constituent, retained austenite, has been found to be present as narrow, elongated laths or as irregular shaped particles along interlath boundaries as well as within the laths. The occurrence of significant amounts of retained austenite has also been documented in A710/modified A710 steels in association with both martensite [12] and acicular ferrite regions [13]. In the present investigation, the only other second phase identified in the quenched alloy was niobium carbide.

Ageing at 605°C for times of 1 or 3 hours leads to:

(i) recovery of the heavily dislocated lath martensitic microstructure;

(ii) nucleation, growth and coarsening of ε-Cu copper precipitates;

(iii) nucleation and growth of cementite possibly by the decomposition of the retained austenite into ferrite and carbide.

The precipitates of ε-copper in the aged material display the commonly observed K-S relationship with the ferrite as noted previously in Fe-Cu alloys [9] and in several Fe-Cu-Ni alloys [10,11].

With respect to (iii), it is expected that the tempering of the martensite would lead to some precipitation of carbides relieving the ferrite of excess carbon. However, cementite particles are very seldom observed in the HSLA-100 alloy. As for the possibility of retained austenite

transforming to ferrite + carbide, the experimental evidence suggests the austenite is stabilized and this kind of a reaction is suppressed in this steel during tempering for times up to 3 hours at 605°C. Indeed, it is possible that excess carbon from the ferrite would partition to the retained austenite which in turn becomes further stabilized. The absence of a notable degree of cementite precipitation in the aged material may be considered to support this view.

CONCLUSIONS

The present study leads to the following conclusions:

(i) the as-quenched microstructure in the 0.04 wt% C HSLA-100 alloy consists of a lath martensitic structure;

(ii) the principal second phase constituent in retained austenite which remains stable after 3 hours of ageing at 605°C;

(iii) tempering leads to recovery of the microstructure resulting in a decrease in hardness;

(iv) the heavily dislocated substructure as well as the increased lath boundary area in the quenched material provides nucleation sites for the ε-Cu precipitates;

(v) tempering leads to formation of a low number density of cementite precipitates, mostly along grain or packet boundaries. Cementite formation via retained austenite decomposition appears to be very sluggish.

ACKNOWLEDGEMENTS

The authors are grateful to the Office of Naval Research, Grant No. N00014-89-3-1958 for financial support. Dr. M. Vassilaros of the David Taylor Research Center is also thanked for the provision of materials and for helpful discussions.

REFERENCES

1. L. G. Kvidahl, "An Improved High Yield Strength Steel for Shipbuilding", **Welding Journal**, Vol . 64, pp. 42-48 (1985).

2. A. D. Wilson, "High Strength, Weldable Precipitation Aged Steels", **J. Metals**, Vol. 39, pp. 36-38 (1987).

3. T. L. Anderson, J. A. Hyatt and J. C. West, "The Benefits of New High-Strength Low-Alloy (HSLA) Steels", **Welding Journal**, Vol. 66, pp. 21-26 (1987).

4. G. R. Speich and T. M. Scoononer, "Continuous-Cooling-Transformation Behavior and Strength of HSLA-80 (A710) Steel Plates", **Processing, Microstructure and Properties of HSLA Steels**, The Metals Society, Warrendale, pp. 263-286 (1988).

5. T. W. Montemarano, B. P. Sack, J. P. Gudas, M. G. Vassilaros, and H. H. Vanderveldt", High Strength Low Alloy Steels, Naval Construction", **J. Ship Prod.**, Vol. 2, pp. 145-162 (1986).

6. J. Gordine, "Weldability of a Ni-Cu-Cb Line-Pipe Steel", **Weld. Res. Supplement**, pp. 179-185 (1977).

7. A. P. Coldren and T. B. Cox, "Development of 100 ksi Yield Strength HSLA Steel", DTNSRDC/SME-Cr-07-87, (24 June 1987).

8. A. D. Wilson, E. G. Hamburg, D. J. Colvin, S. W. Thompson, and G. Krauss, "Properties and Microstructures of Copper Precipitation Aged Plate Steels", **Microalloyed HSLA Steels**, American Society of Metals, Cleveland, pp. 259-275 (1988).

9. P. R. Howell, R. A. Ricks, J. V. Bee and R. W. K. Honeycombe, "Precipitate Orientations in Isothermally Transformed Iron-base Alloys", **Phil. Mag A**, Vol. 41, pp. 165-175 (1980).

11. R. A. Ricks, P. R. Howell and R. W. K. Honeycombe, "Formation of Supersaturated Ferrite During Decomposition of Austenite in Iron-Copper an Iron-Copper-Nickel Alloys", **Metal Sci.** Vol. 14, 562-568 (1980).

12. S. W. Thompson, D. J. Colvin, and G. Krauss, "On the Bainitic Structure Formed in a Modified A710 Steel", **Scripta Met.**, Vol. 22, pp. 1069-1074 (1988).

13. S. W. Thompson, D. J. Colvin, and G. Krauss, "Continuous Cooling Transformations and Microstructures in a Low-Carbon High-Strength Low-Alloy Plate Steel", **Met. Trans. A**, Vol. 21A, pp. 1493-1507 (1990).

Table 1. Chemical Composition of the Steel (wt%)

C	Mn	P	S	Si	Cu	Ni	Cr	Mo	Al	Nb
0.04	0.82	0.014	0.002	0.32	1.59	3.45	0.58	0.51	0.03	<0.05

FIGURE CAPTIONS

Figure 1. Optical Micrograph of the as-quenched HSLA-100 alloy revealing a fully lath martensitic structure.

Figure 2. TEM bright field (BF) image of laths within a packet in the as-quenched material.

Figure 3. Centered dark field (CDF) image of retained austenite formed by the austenite (002) reflection.

Figure 4a. CDF image of niobium carbide precipitates in the quenched steel.

b. Selected area diffraction (SAD) pattern showing ferrite and NbC reflections.

Figure 5a. BF image of the acicular laths in the 3-hr aged material.

b. CDF of area in (a) illustrates laths of a common orientation.

Figure 6a. CDF image of ε-copper precipitates after 1 hr ageing at 605°C. Image formed by $(002)_{\gamma/\varepsilon\text{-Cu}}$.

b. Indexed SAD pattern from the area in (a). Subscripts: a-austenite, F-ferrite, e-epsilon copper. $[\bar{1}10]_{a/e}$ and $[1\bar{1}1]_F$ zones.

Figure 7. CDF image of ε-copper after 3 hours ageing at 605°C indicates coarse particles.

Figure 8a. BF image of area from the 3-hr aged material revealing intra lath retained austenite in the recovered microstructure.

b. CDF image of irregularly shaped retained austenite particles

c. Indexed convergent beam pattern from one of the austenite particles: $[\bar{1}10]$ zone.

Figure 1. Optical Micrograph of the as-quenched HSLA-100 alloy revealing a fully lath martensitic structure.

Figure 2. TEM bright field (BF) image of laths within a packet in the as-quenched material.

Figure 3. Centered dark field (CDF) image of retained austenite formed by the austenite (002) reflection.

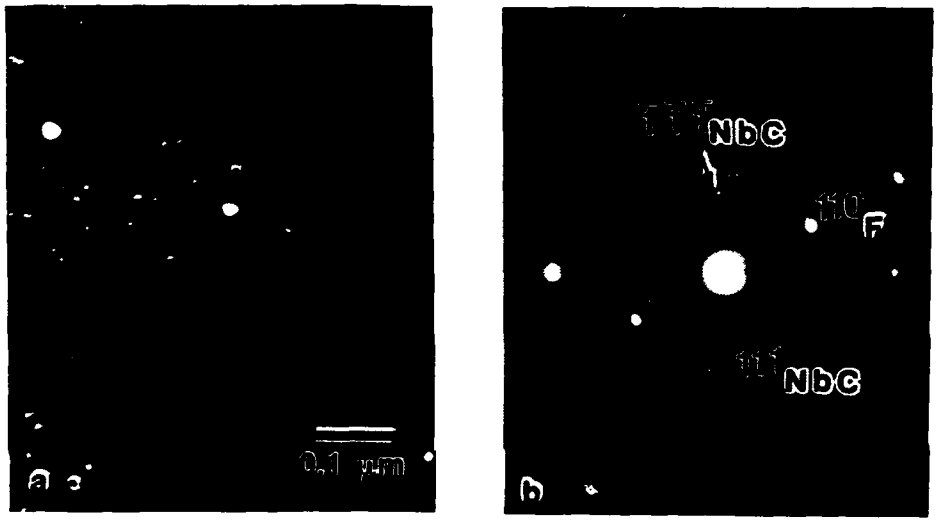

Figure 4a. CDF image of niobium carbide precipitates in the quenched steel.

b. Selected area diffraction (SAD) pattern showing ferrite and NbC reflections.

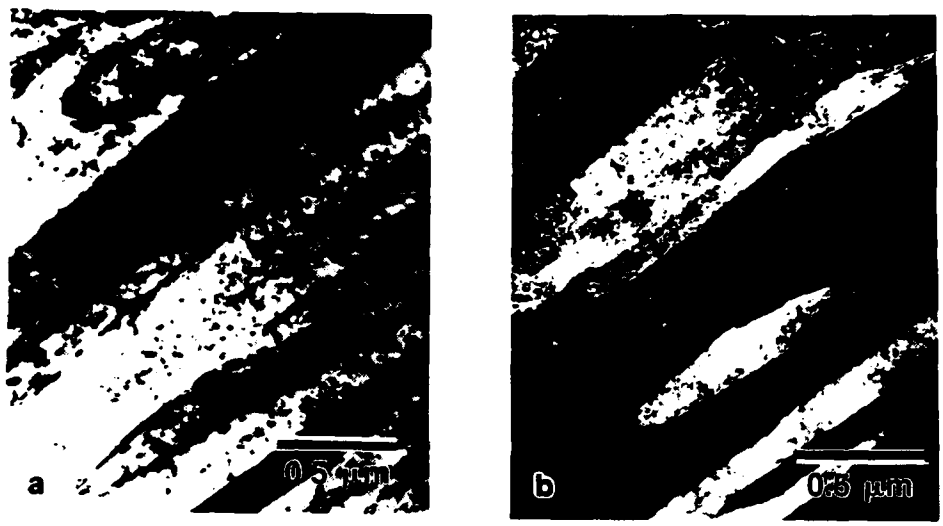

Figure 5a. BF image of the acicular laths in the 3-hr aged material.

b. CDF of area in (a) illustrates laths of a common orientation.

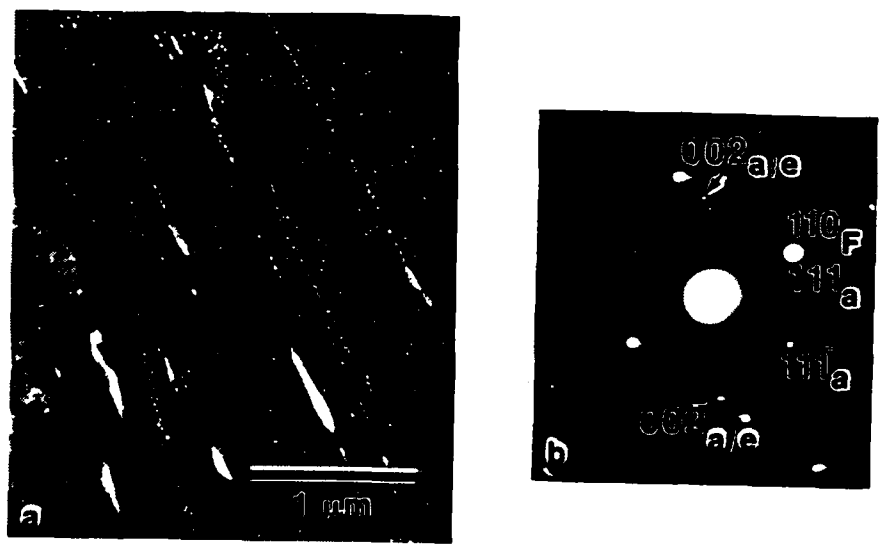

Figure 6a. CDF image of ε-copper precipitates after 1 hr ageing at 605°C. Image formed by $(002)_{\gamma/\varepsilon\text{-Cu}}$.

b. Indexed SAD pattern from the area in (a). Subscripts: a-austenite, F-ferrite, e-epsilon copper. $[\bar{1}10]_{a/e}$ and $[1\bar{1}1]_F$ zones.

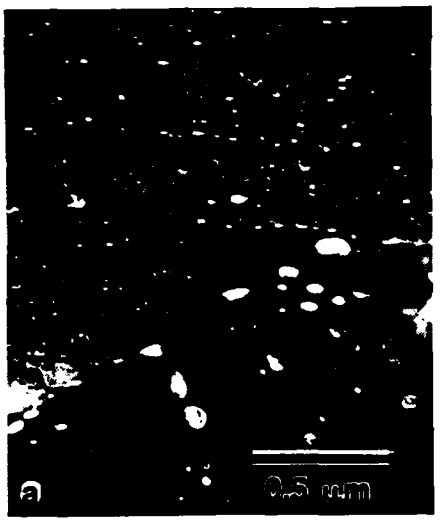

Figure 7. CDF image of ε-copper after 3 hours ageing at 605°C indicates coarse particles.

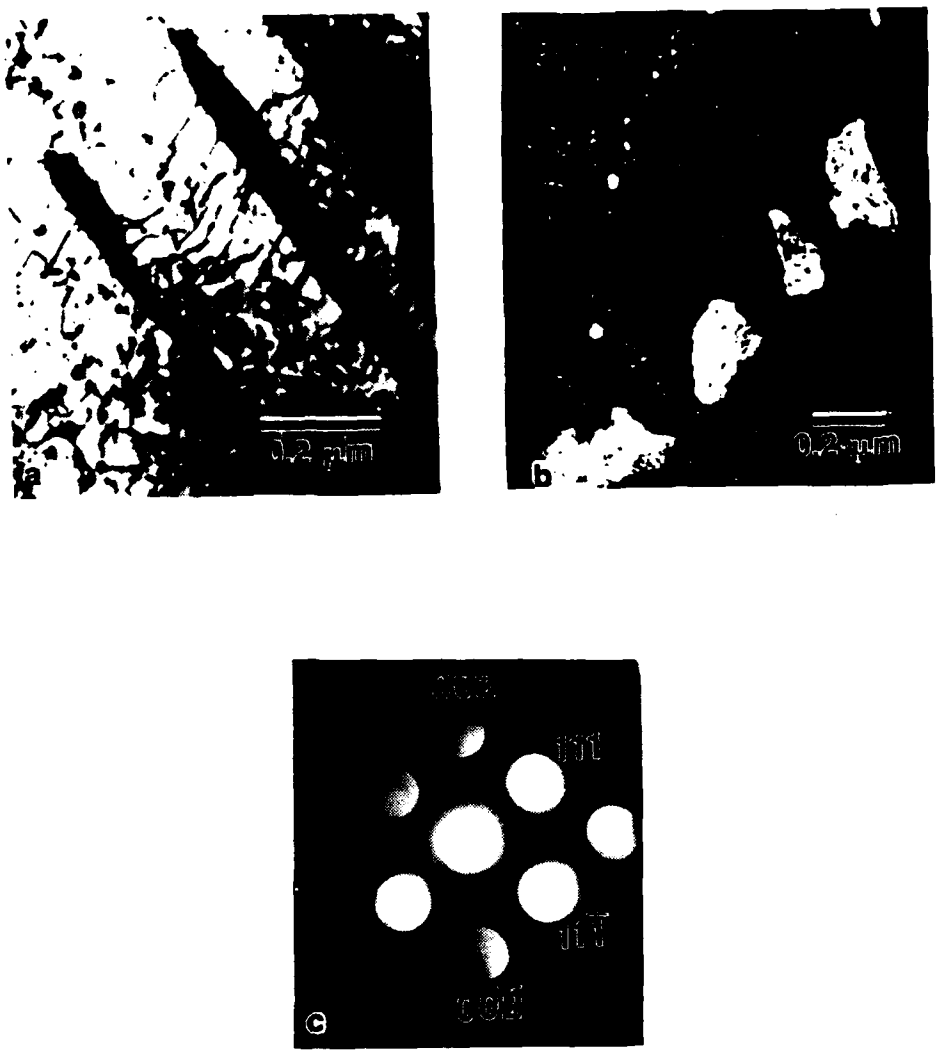

Figure 8a. BF image of area from the 3-hr aged material revealing intra lath retained austenite in the recovered microstructure.

b. CDF image of irregularly shaped retained austenite particles

c. Indexed convergent beam pattern from one of the austenite particles: [$\bar{1}$10] zone.

To be published in : " *Metallography : 75 Years Later* "
ed. G. F Vander Voort. ASTM,Philadelphia, PA

THE APPLICATION OF TRANSMISSION ELECTRON MICROSCOPY TO THE STUDY 0F A LOW CARBON STEEL: HSLA-100

Rajan Varughese, Department of Materials Science and Engineering, The Pennsylvania State University, University Park, PA 16802, U.S.A.

Paul R. Howell, Department of Materials Science and Engineering, The Pennsylvania State University, University Park, PA 16802, U.S.A.

ABSTRACT: Transmission electron microscopy (TEM) together with scanning electron microscopy (SEM) and optical microscopy have been employed to analyze the microstructures that develop in a copper-containing, low carbon (0.04 wt%) HSLA- 100 alloy. Specifically, the martensitic structures that develop in the simulated, coarse-grained heat affected zones (HAZs) have been examined and compared with those which develop in the base plate during conventional quenching from the austenitic phase field. It has been shown that the lath martensitic packet size is increased dramatically in the HAZ as compared with the base plate. In addition, considerably more retained austenite is found in the HAZ. No evidence for the so-called granular bainite microconstituent has been found in either material. However, for cooling rates somewhat less than that experienced in the coarse-grained HAZ, a microconstituent which we term granular ferrite has been documented.

Finally, the effect of tempering on the martensite in the base plate has been examined. As soon as they are observable, the copper particles can be identified as fcc ε-Cu.

ABSTRACT: Transmission electron microscopy (TEM) together with scanning electron microscopy (SEM) and optical microscopy, have been employed to analyze the microstructures that develop in a copper-containing, low-carbon (0.04 wt%) HSLA- 100 alloy. Specifically, the martensitic microstructures which develop in the simulated, coarse-grained heat affected zones (HAZs) have been examined and compared with those which develop in the base plate during conventional quenching from the austenitic phase field. It has been shown that the lath martensitic packet size is increased dramatically in the HAZ as compared with the base plate. In addition, considerably more retained austenite is found in the HAZ. No evidence for the so-called granular bainite microconstituent has been found in either material. However, for cooling rates somewhat less than that experienced in the coarse-grained HAZ, a microconstituent which we term granular ferrite, has been documented.

Finally, the effect of tempering on the martensite in the base plate has been examined. As soon as they are observable, the copper precipitates can be identified as fcc ε-Cu.

KEYWORDS: steels, martensite, granular bainite, granular ferrite, copper precipitates, welding, heat affected zones, transmission electron microscopy, scanning electron microscopy, light microscopy.

TITLE OF SYMPOSIUM OR TITLE OF ASTM JOURNAL: Metallography: 75 Years Later.

AUTHORS' NAMES:

Rajan Varughese[1] and Paul R. Howell[1]

TITLE OF PAPER:

The Application of Transmission Electron Microscopy to the Study of a Low-Carbon Steel: HSLA-100

AUTHORS' AFFILIATIONS

[1] Research Associate and Professor of Metallurgy, respectively,
Department of Materials Science and Engineering, The Pennsylvania State University,
University Park, PA 16802.

Introduction

This paper is concerned with a metallographic examination of a new class of steels which are designated as HSLA-100. Transmission electron microscopy (TEM), scanning electron microscopy (SEM) and light microscopy have been used to document the predominantly martensitic microstructures that develop in these alloys. HSLA-100 displays superior weldability and hence, as part of an overall investigation of the material, the coarse-grained heat affected zone (HAZ) has been simulated using a Gleeble and analyzed metallographically, primarily by TEM. In addition, the "base plate", which conventionally would be used in the quenched and tempered condition, has been examined and compared with the HAZ.

Previous studies [1,2] have indicated that "granular bainite" might form in these steels. Since the introduction of this terminology [3] to describe certain morphological features found in hardenable steels, it has been often used in the literature, despite the lack of a clear consensus as to the strict nature of this transformation product. In addition, there is no consensus concerning the phases, morphology, and the disposition of the phases that constitute granular bainite [4,5]. Hence, one of the major goals of the study was to obtain unambiguous evidence for the presence(or more likely, the absence) of this microstructural entity. This latter study has also employed cooling rates somewhat less than those experienced in either the HAZ or the quenched base plate.

Experimental Approach

The composition of the experimental material is given in Table 1. For the coarse-grained HAZ studies, 6 mm diameter rods were machined and were weld simulated to a peak temperature of 1320 °C followed by cooling at a rate of 20 °C/sec through the 800 to 500 °C temperature range. This simulation corresponds to a heat input of about 2 kJ/ mm for the plate thickness involved. The simulation was performed on a Gleeble, courtesy of the David Taylor Research Center, Annapolis, MD. In addition, continuous cooling transformation studies were performed on 5 mm thick samples by air cooling from 900 °C. For the present analysis on tempering of the HSLA-100 steel, 6 mm buttons (thickness- 6 mm) were reaustenitized at 900 °C for 15 minutes and then water quenched. The samples were then tempered at 600 °C for times ranging from 30 minutes to 48 hours.

Specimens for light microscopy and SEM were prepared through standard metallographic practices [6] and were etched in nital or a mixture of nital and picral.Thin foil specimens for TEM analysis were prepared by first grinding 1-mm thick slices on a 400/ 600 grit SiC paper to a thickness of 75-100 μm. 3 mm diameter discs were subsequently punched and further ground to 35- 50 μm thickness on 600 grit SiC paper. The discs were then electropolished to electron transparency in a twin-jet electropolishing unit using an electrolytic mixture consisting of 95 % acetic acid and 5 % perchloric acid at room temperature. TEM examinations were carried out using a Philips EM420T at an accelerating voltage of 120 kV.

Results and Discussion

This section is organized as follows. The results of the coarse-grained HAZ simulation are presented first and then compared with the quenched base plate. The tempering studies will then follow, and finally, the microstructure that develops in the HAZ and the quenched base plate will be compared with microstructures that develop during somewhat slower cooling rates from the austenitic phase field.

The Microstructure of the Coarse-Grained HAZ

The microstructure of the simulated coarse-grained HAZ (peak temperature: 1320 °C and cooling rate approx. 20 °C per sec) consisted of very large packets (≈50 μm in diameter) of lath martensite as shown in figures 1a,b. The laths are typically 0.2- 0.4 μm wide. Reference to figure 1b shows that what might be termed " granular features" are present (arrowed).

TEM examination of the HAZ confirmed the presence of lath martensite (eg. see figure 2a) and it can also be seen that there are interlath films which appear dark in the bright field (BF) image. Centered dak field (CDF) images of the latter regions (eg. see figures 2b,c) show that these interlath films are retained austenite (figures 2b and c were imaged using an 002 austenite reflection- see also figure 8c). Reference to figures 2b, c also shows that ε-Cu precipitation is absent in the CDF images (since both γ and ε- Cu are related to the ferrite by the Kurdjumov-Sachs OR [7, 8], then a fraction of any ε- copper that might be present should also be illuminated in the austenite CDF image). This is not surprising, considering the relatively rapid cooling rate. However, the possibility of Cu-rich G.P. zones being present cannot be discounted. Finally, no evidence for granular bainite was found, and the occasional, large ferritic regions that were observed were found to be twinned as shown in the BF- twin CDF image pair of figure 3. Hence, it can be concluded that the microstructure in the HAZ is comprised of lath martensite together with retained austenite.

The Microstructure of the Quenched Base Plate

Details of the material which had been reaustenitized at 900 °C and quenched are to be published elsewhere [9]. However, for the sake of completeness and to facilitate a comparison with the HAZ, a brief description follows. Figures 4 and 5 are a light micrograph and BF TEM image, respectively, of the quenched material. The quenched material is fully martensitic, consisting primarily of fine laths with widths of the order of 0.1-0.2 μm and several microns in length. Generally, this length is limited either by the block dimension or the packet size. At this point it can be noted that the laths in the HAZ could be as long as 50 μm which was the

approximate packet size. Now, reference to figure 4 reveals a number of regions which are lightly etched and again could be identified as granular bainite. However, TEM analysis provided no evidence for such a microstructure and the only other microconstituent found in the quenched material was retained austenite, located primarily at the interlath boundaries as also noted in other low carbon steels containing nickel and chromium[10]. In contrast to the HAZ, the volume fraction of retained austenite was very small. In common with the HAZ, some large internally twinned regions were observed occasionally. These large internally twinned martensitic units are occasionally observed in low carbon steels [11].

The Effect of Tempering on the Quenched Base Plate

Figures 6 and 7 are light micrographs of samples that had been tempered for 2 hours and 48 hours, respectively, at 600 °C. At these magnifications, there seems to be little difference in the two materials. However, TEM examinations reveal that substantial microstructural changes occur during extended tempering treatments.

After 3 hours ageing (figures 8a,b), the lath structure is still preserved and a fine dispersion (≈ 25 nm in diameter) of ε-Cu has developed both, on the lath boundaries and within the laths. The CDF image of copper precipitates seen in figure 8b has been formed by the combined (002) γ/ ε-Cu reflection as shown in figure 8c (austenite and ε-Cu both being fcc and have similar lattice parameters, the 002 diffraction spots coincide). The CDF image in figure 8b also reveals the presence of stabilized austenite in the microstructure after ageing. After 10 hours of ageing, the lath structure is replaced partially by equiaxed ferrite (figure 9a) although certain regions still retain vestiges of the lath structure (figure 10). CDF images of the precipitates formed by the (002) copper reflection confirms their identity as ε-Cu. Comparison of figures 9 and 10 with that of figure 8 shows that the copper precipitates have coarsened considerably after 10 hours and many of the larger intragranular particles are assuming a rod-like morphology. After 48 hours ageing the dominant ferritic morphology is equiaxed (figure 11) although, in common with the 10-hour aged

material, certain regions still retain a lath-like morphology (figure 12). Reference to figure 11 shows a number of coarse ε-Cu precipitates on the grain boundaries.

The Microstructure of Air-Cooled Samples of the Base Plate

Specimens which were reaustenitized at 900 °C and cooled at 7.5 °C per sec were examined in order to (hopefully) develop ferrite/ martensitic microstructures which could correspond to what has been termed "granular bainite". Reference to figure 13 shows that a dual phase, ferrite plus martensite, microstructure develops. The martensite was found at the equiaxed ferrite grain boundaries, and somewhat interestingly within the ferrite grains (figures 14 a and b). This latter microconstituent, ferrite plus entrapped pools of martensite could be termed granular bainite. However, we would argue that granular ferrite is a more appropriate designation since this microconstituent, predominantly ferrite plus martensite, does not conform to either of the current definitions of bainite which are (for steels):

(i) a non-lamellar aggregate of ferrite plus cementite [12];

and (ii) a lath or plate-like ferritic product which forms by shear [13].

At this point, it should be pointed out that, in the present investigation, microstructures similar to that presented in figures 13 and 14 have not been found in either the HAZ or the quenched base plate. This again reinforces our claim that these latter regions are predominantly lath martensitic together with retained austenite as the second phase constituent.

Conclusions

The major findings of the present investigation are as follows:

(1) The coarse-grained HAZ transforms to a coarse lath martensite during cooling. Austenite is retained as thin interlath films.

(2) The quenched base plate is also comprized of lath martensite, but on a finer scale. Little retained austenite was observed.

(3) No granular bainite/ ferrite was found in either the HAZ or the quenched base plate.

(4) Tempering the quenched base plate led to the development of a dispersion of ε-Cu. The lath structure was generally replaced by a more equiaxed ferritic structure.

(5) Granular ferrite was found in the air-cooled sample. It has been argued that the designation - ferrite, is far more appropriate than that which has been used heretofore - bainite.

Acknowledgements

The authors gratefully acknowledge the support of The Office of Naval Research- Grant Number N00014- 89- J1958.

References

[1] Wilson, A.D., Hamburg, E.G., Colvin, D.J., Thompson, S.W.,and Krauss, G., in Microalloyed HSLA Steels (Proceedings Microalloying' 88), ASM, 1988, p.259.

[2] Thompson, S.W., Colvin, D.J., and Krauss, G., Scripta Metallurgica, Vol.22, 1988, p.1069.

[3] Habraken, L.J. and Economopoulos, M., in Transformation and Hardenability in Steels, Climax Molybdenum Company, Michigan, 1967, p.69.

[4] Bramfitt, B.L., and Speer, J.G., Metallurgical Transactions A, Vol.21A, 1990, p.817.

[5] Ohtani, H.,Okugachi, S.,Fujishiro, Y.,and Ohmori, Y., Metallurgical Transactions A, Vol.21A, 1990, p.877.

[6] Vander Voort, G., Metallography- Principles and Practices, McGraw - Hill. Inc., 1984.

[7] Honeycombe, R.W.K., in Phase Transformations in Ferrous Alloys (eds. A.R.Marder and J.I.Goldstein), The Metallurgical Society of AIME, 1984, p. 259.

[8] Howell, P.R., Ricks, R. A.,and Honeycombe, R.W.K., Journal of Materials Science, Vol.15, 1980, p.376.

[9] Varughese, R. and Howell, P.R., to be published.

[10] Thomas, G., Metallurgical Transactions A, Vol.9A, 1978, p.439.

[11] Wayman, C.M., in Phase Transformations in Ferrous Alloys (eds. A.R.Marder and J.I.Goldstein), The Metallurgical Society of the AIME, 1984, p.49.

[12] Aaronson, H.I. et al., Metallurgical Transactions A, Vol.21A, 1990, p.1343.

[13] Olson, G.B. et al., Metallurgical Transactions A, Vol.21A, 1990, p.805.

TABLE 1--Chemical composition of the HSLA-100 steel (weight percent)

C	Mn	P	S	Si	Cu	Ni	Cr	Mo	Al	Nb
0.04	0.82	0.014	0.002	0.32	1.59	3.45	0.58	0.51	0.03	0.03

Figure Captions

FIG. 1-- Microstructure of the coarse-grained HAZ (simulated for a weld heat input of 2 kJ/mm) in the HSLA-100 alloy. Cooling rate ≈ 20 $^{o}C\ s^{-1}$. (a) Light micrograph of the basic martensitic structure, and (b) SEM micrograph of the lath structure. Narrow, elongated interlath constituents are also present.

FIG. 2-- (a) TEM bright field (BF) image of the lath microstructure; (b, c) Centered dark field (CDF) images of retained austenite ((002) austenite reflections).

FIG. 3-- (a) TEM BF image of a large martensitic grain which contains fine-scale twins; (b) corresponding twin CDF image.

FIG. 4-- Light micrograph of the quenched base plate.

FIG. 5-- BF image of the lath martensite. Fine niobium carbide precipitates are present.

FIG. 6-- Light micrograph of the base plate after tempering for 2 hrs at 600 ^{o}C.

FIG. 7-- Light micrograph of the base plate after tempering for 48 hrs.

FIG. 8-- (a) TEM BF image of the lath structure and copper precipitates, (b) austenite / ε-Cu CDF image, and (c) Selected area diffraction pattern (SADP) of figures 8 a,b. The (002) reflection was used to form figure 8b.

FIG. 9-- (a) TEM BF image of coarsened copper precipitates after 10 hrs ageing. (b,c) CDF image formed with the (002) ε-Cu reflection.

FIG. 10-- BF image of the lath-like microstructure after 10 hrs of ageing.

FIG. 11-- Coarse precipitates of copper on the grain boundaries after 48 hours ageing.

FIG. 12-- BF image of the 48-hr aged material. Remnants of a lath morphology are obsrved.

FIG. 13-- (a) Light micrograph of specimen cooled at 7.5 $^{o}C\ s^{-1}$. A granular morphology is present. (b) TEM BF image: the structure is a dual phase, consisting of equiaxed ferrite and martensite.

FIG. 14-- Intragranular pools of martensite in the air-cooled material (7.5 $^{o}C\ s^{-1}$) : (a) BF and (b) corresponding martensite CDF image.

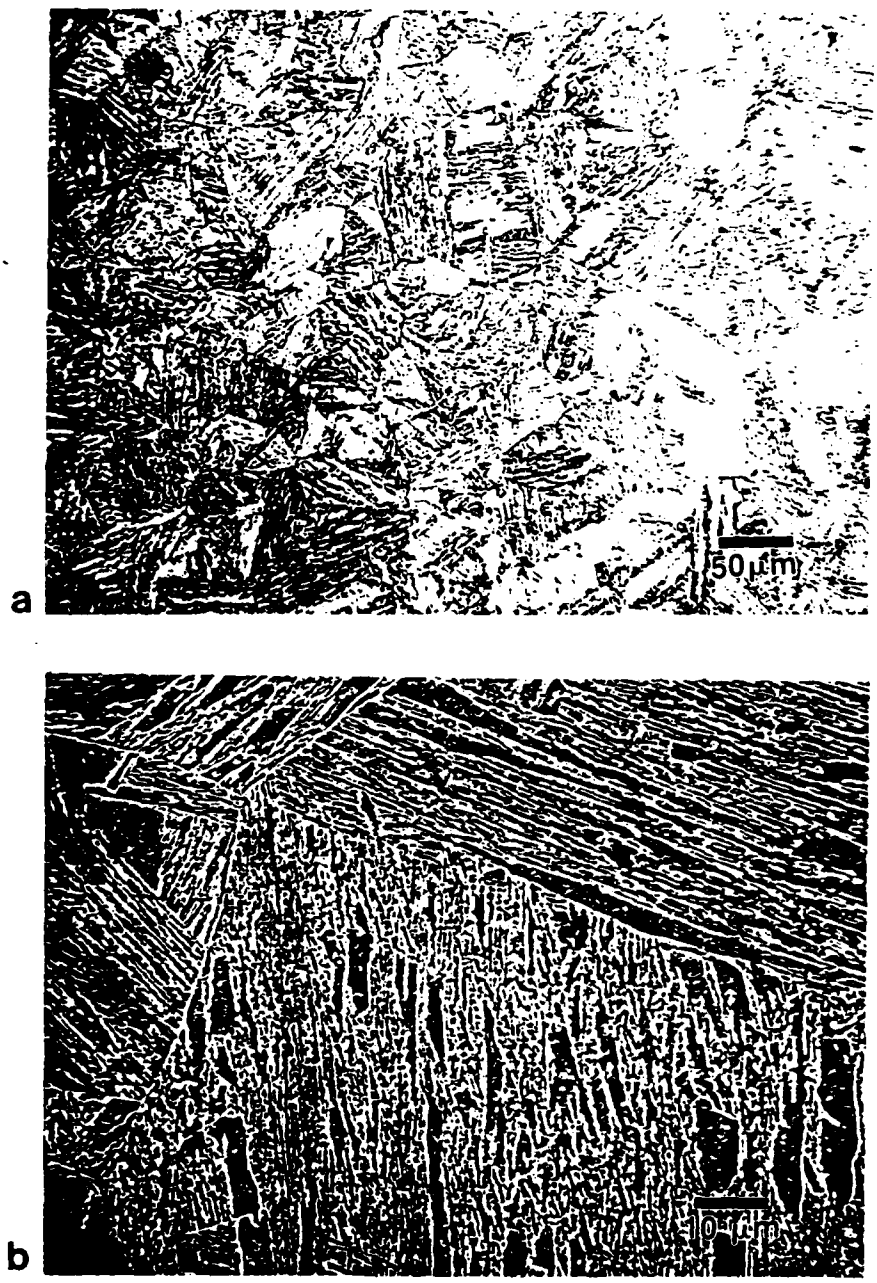

FIG. 1-- Microstructure of the coarse-grained HAZ (simulated for a weld heat input of 2 kJ/mm) in the HSLA-100 alloy. Cooling rate ≈ 20 $^{o}C\ s^{-1}$. (a) Light micrograph of the basic martensitic structure, and (b) SEM micrograph of the lath structure. Narrow, elongated interlath constituents are also present.

FIG. 2-- (a) TEM bright field (BF) image of the lath microstructure; (b, c) Centered dark field (CDF) images of retained austenite ((002) austenite reflections).

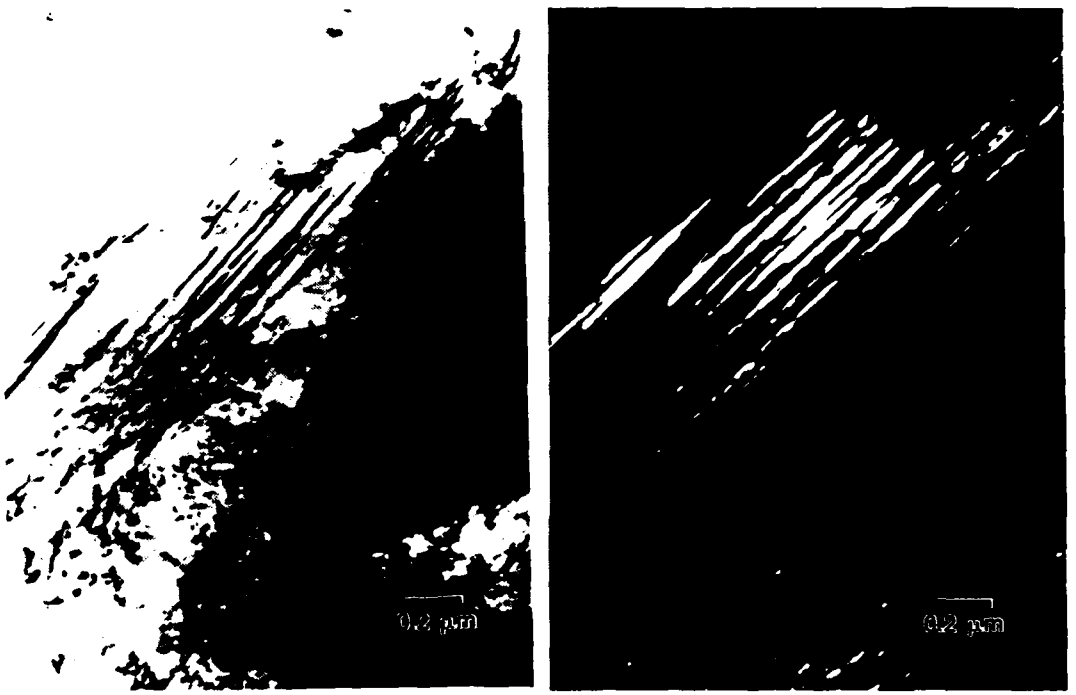

FIG. 3-- (a) TEM BF image of a large martensitic grain which contains fine-scale twins; (b) corresponding twin CDF image.

FIG. 4-- Light micrograph of the quenched base plate.

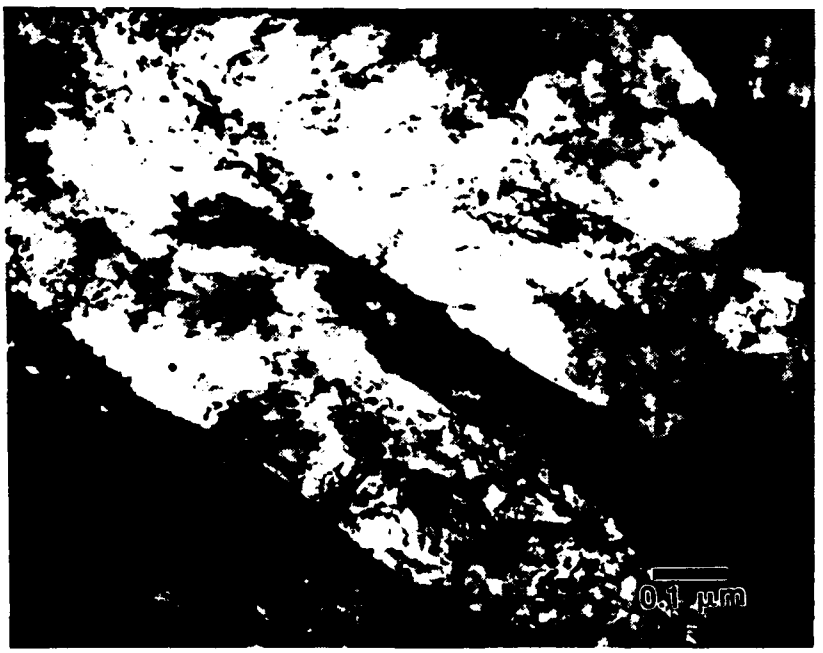

FIG. 5-- BF image of the lath martensite. Fine niobium carbide precipitates are present.

FIG. 6-- Light micrograph of the base plate after tempering for 2 hrs at 600 °C.

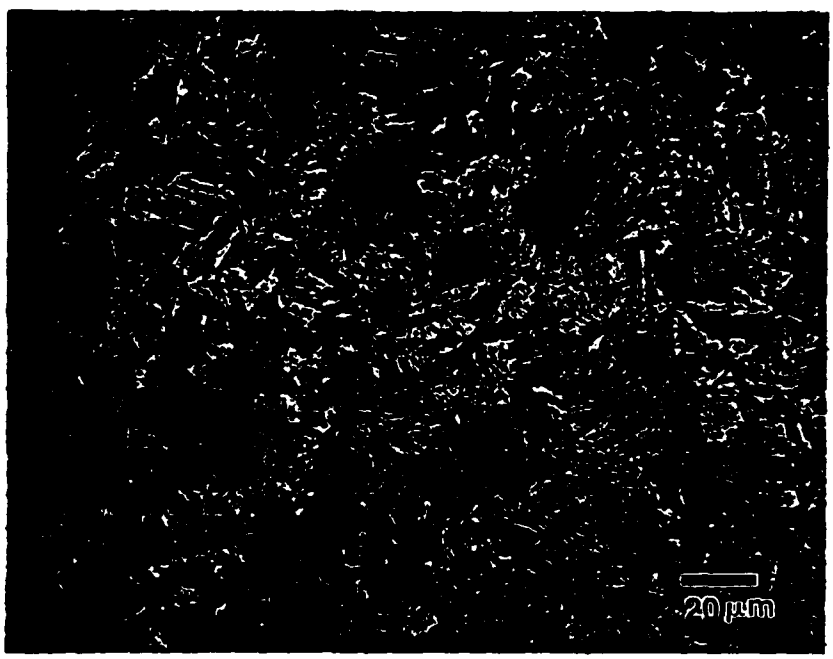

FIG. 7-- Light micrograph of the base plate after tempering for 48 hrs.

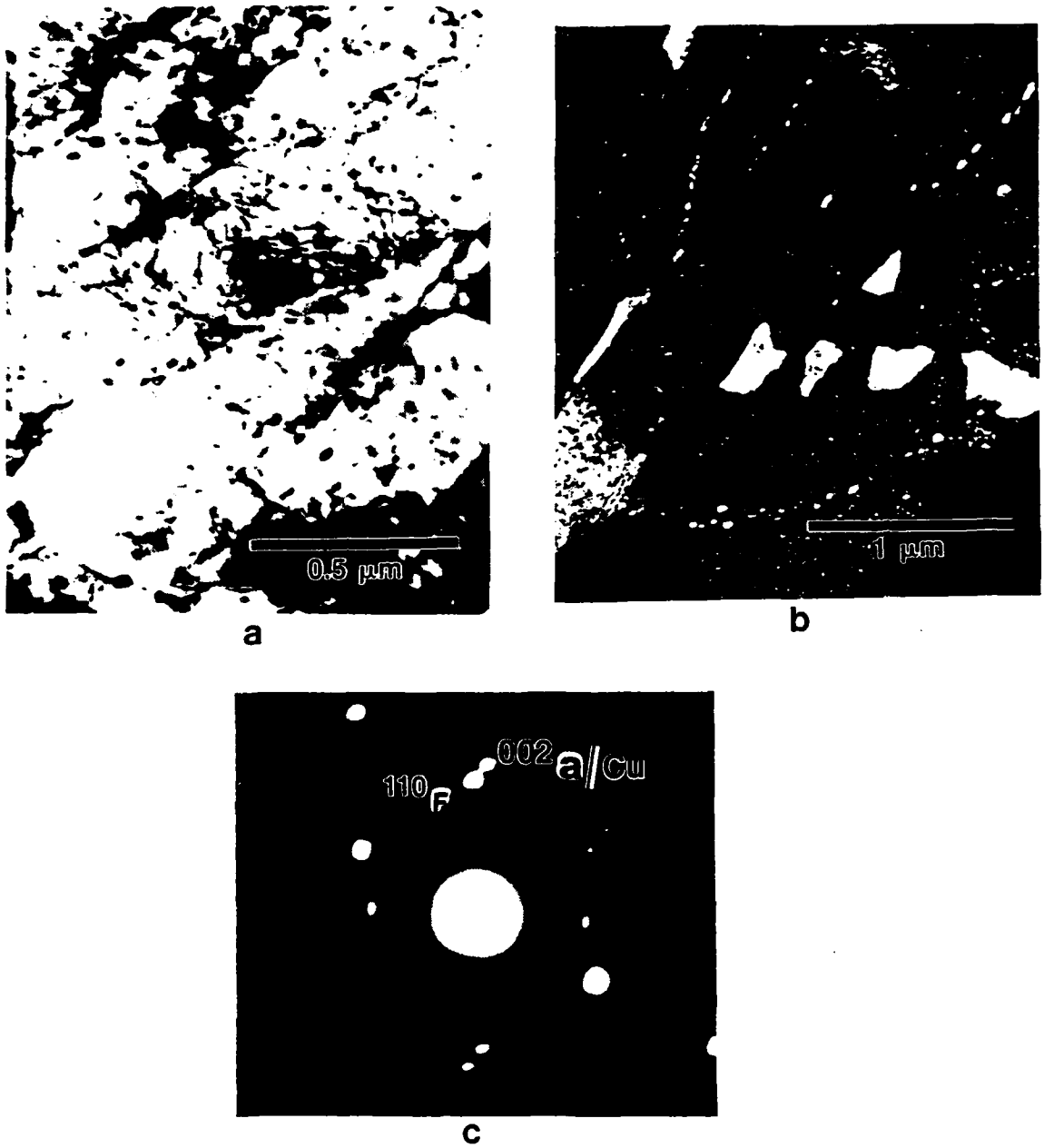

FIG. 8-- (a) TEM BF image of the lath structure and copper precipitates, (b) austenite / ε-Cu CDF image, and (c) Selected area diffraction pattern (SADP) of figures 8 a,b. The (002) reflection was used to form figure 8b.

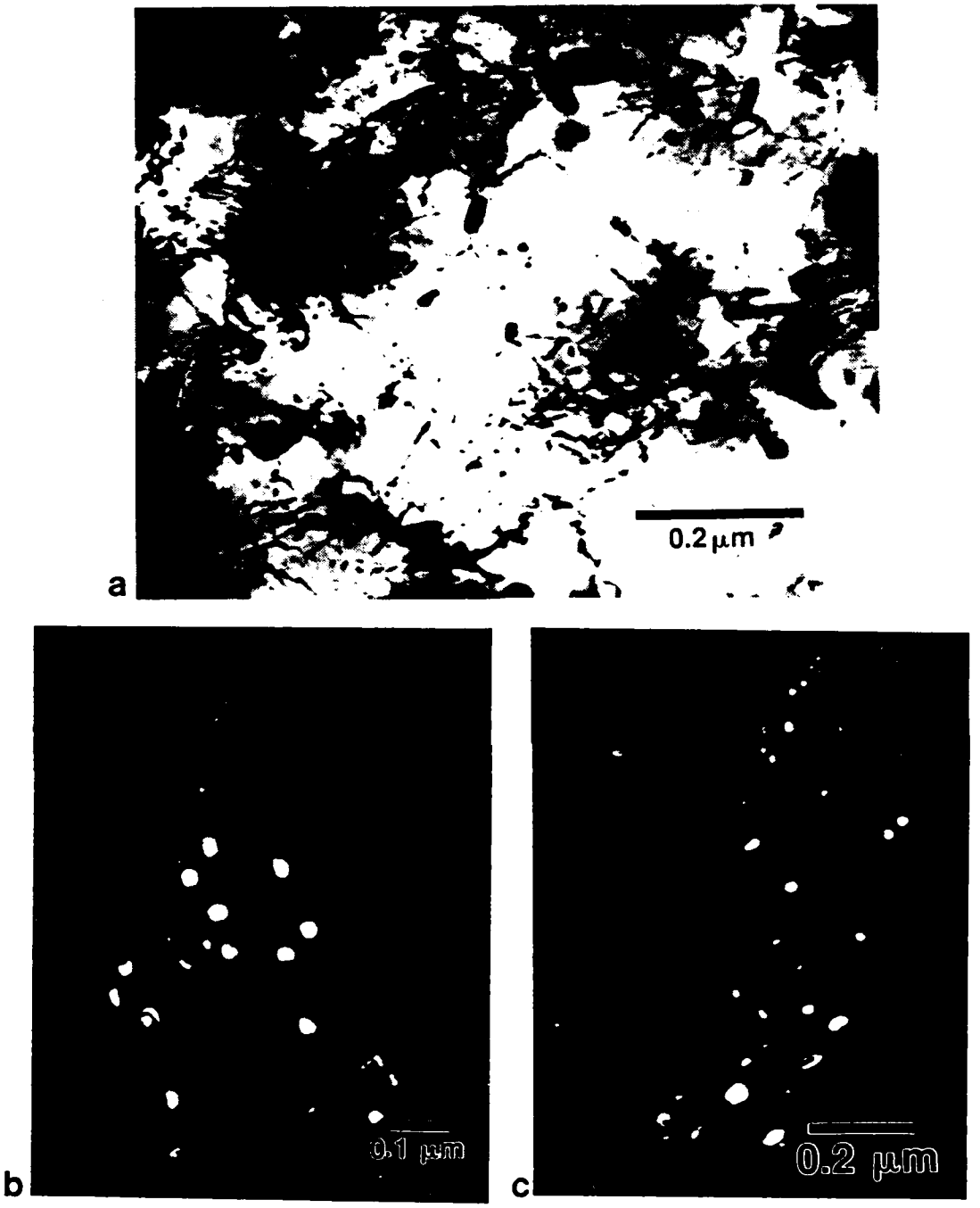

FIG. 9-- (a) TEM BF image of coarsened copper precipitates after 10 hrs ageing. (b,c) CDF image formed with the (002) ε-Cu reflection.

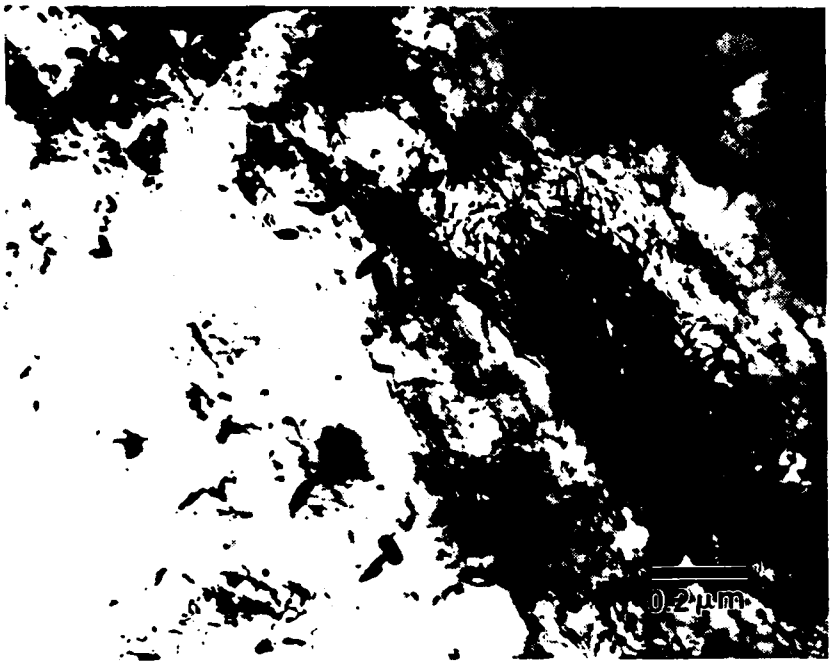

FIG. 10-- BF image of the lath-like microstructure after 10 hrs of ageing.

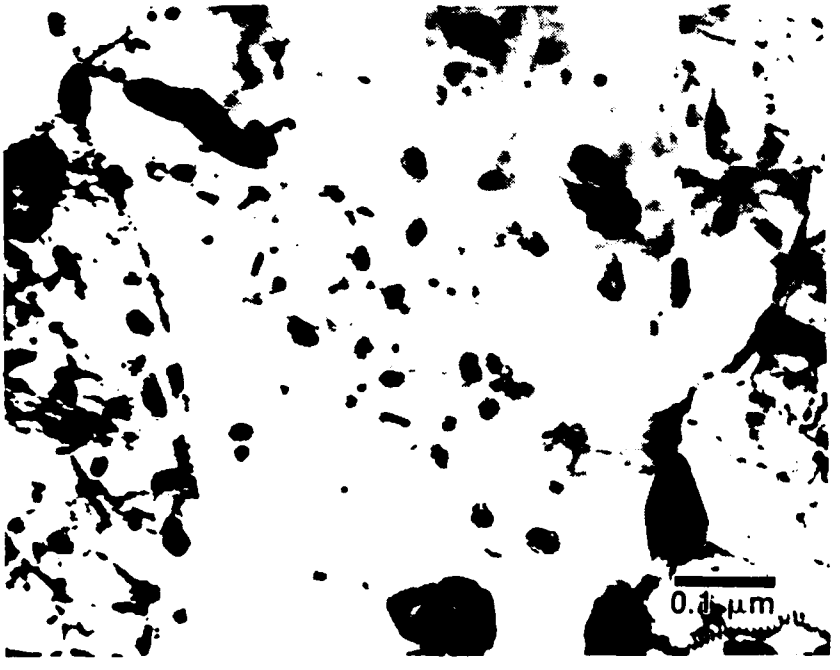

FIG. 11-- Coarse precipitates of copper on the grain boundaries after 48 hours ageing.

FIG. 12-- BF image of the 48-hr aged material. Remnants of a lath morphology are obsrved.

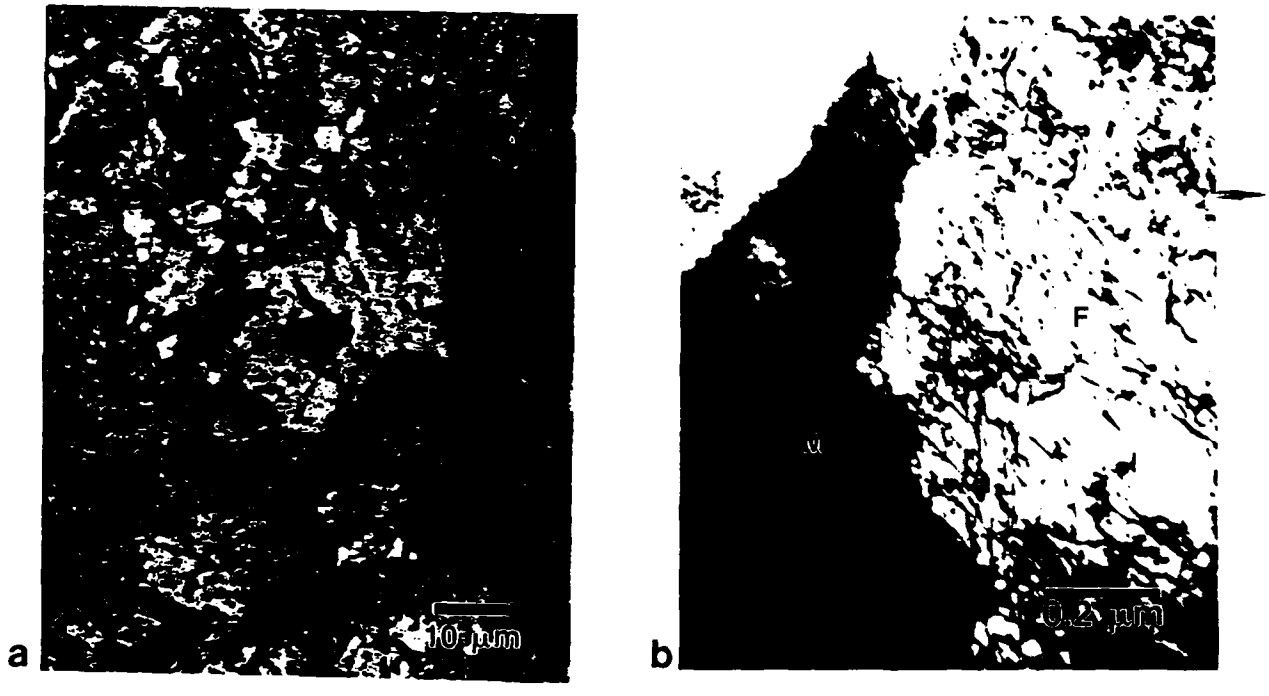

FIG. 13-- (a) Light micrograph of specimen cooled at 7.5 $^{o}C\ s^{-1}$. A granular morphology is present. (b) TEM BF image: the structure is a dual phase, consisting of equiaxed ferrite and martensite.

FIG. 14-- Intragranular pools of martensite in the air-cooled material (7.5 °C s^{-1}) : (a) BF and (b) corresponding martensite CDF image.

To be submitted to : " *Journal of Materials Science* "

THE INTERACTION BETWEEN PROEUTECTOID FERRITE AND AUSTENITE DURING THE ISOTHERMAL TRANSFORMATION OF TWO LOW CARBON STEELS - A NEW MODEL FOR THE DECOMPOSITION OF AUSTENITE

J.-W Lee,[1] S.W. Thompson[2] R. Varughese[3] and P.R. Howell[3]

[1]Thomas J. Watson Research Center, P.O. Box 218, Yorktown Heights, NY 10598

[2]Advanced Steel Processing and Products Research Center, Department of Metallurgical Engineering, Colorado School of Mines, CO 80401

[3]Department of Materials Science and Engineering, The Pennsylvania State University University Park, PA 16802

ABSTRACT

Both scanning electron microscopy (SEM) and transmission electron microscopy (TEM) have been employed to examine the austenite to proeutectoid ferrite and ferrite/carbide reactions in two low carbon (0.04 wt%) steels. It is demonstrated that proeutectoid ferrite (both polygonal and Widmanstätten) can "partition" the prior austenite grains into several smaller units or pools. It is also shown that prior to the initiation of the pearlite reaction, ferrite grain growth can occur. The pools of austenite exert a Zener-like drag force on the migrating ferrite grain boundaries. However, the ferrite boundaries can eventually break away and small pools of austenite become completely embedded in single proeutectoid ferrite grains. Subsequently, these small pools of austenite transform to discrete regions of cementite, together with epitaxial ferrite. Conversely, certain small pools remain in contact with the ferrite grain boundaries and it is considered that transformation of these latter pools will eventually lead to the formation of massive films of cementite at the ferrite grain boundaries. Larger pools of austenite prevent ferrite boundary breakaway, and these latter, austenitic regions eventually transform to pearlite.

1. INTRODUCTION

In a previous study of two low carbon (0.04wt%) lamination steels, the isothermal decomposition of austenite was investigated, [1]. In [1], the formation of pearlite and massive films of cementite was considered in detail. However, the proeutectoid ferrite reaction received little attention., A subsequent re-examination of the early stages of the decomposition of austenite (i.e. prior to the onset of the pearlite reaction) in these alloys has revealed a complex distribution of the remaining pools of austenite. For example, neither the size nor the location of the austenite pools could be reconciled with the conventional picture, that proeutectoid ferrite nucleates on the austenite grain boundaries and forms a skeleton at the prior austenite grain boundaries: the pearlite reaction then occurs when the remaining austenite attains the eutectoid composition.

In light of the above, this paper is concerned primarily with the proeutectoid ferrite reaction in two low carbon lamination steels. In particular, the interaction between proeutectoid ferrite and the remaining pools of austenite is documented. From this, new models for the decomposition of austenite are presented. These models can successfully account for the observation of both films of cementite at ferrite grain boundaries and of discrete precipitates of cementite within the ferritic matrix.

2. EXPERIMENTAL

The experimental materials were obtained from Inland Steel in the form of hot rolled strip, 2.5mm thickness. The compositions of these steels are given in Table 1. Specimen materials were austenitized at 1000°C for five minutes and isothermally transformed in a salt bath followed by iced brine quenching. Details of the transformation temperatures and times are given in Lee et al [1]. For both steels, the austenite grain size was approximately 100 μm.

Specimens for scanning electron microscopy (SEM) were prepared using standard techniques, etched in 2% nital and examined using an I.S.I. Super III A operating at

25kV. Specimens for transmission electron microscopy (TEM) were obtained by electropolishing in a solution consisting of 5% perchloric acid in glacial acetic acid at room temperature and at a potential of 35V. TEM was performed using either a Philips EM 300 operating at 100kV or a Philips EM 420T operating at 120kV. Phase identification employed both selected area diffraction (SAD) patterns and low camera length (LCL) convergent beam electron diffraction (CBED) patterns. LCL-CBED patterns were employed for e.g., the identification of small austenite particles in that:

(i) Kikuchi lines are more readily visible in CBED patterns and

(ii) reflections from Higher Order Laue Zones (HOLZs) can be analyzed as follows:

The radius of the First Order Laue Zone, FOLZ, ($|\underline{G}|$) as measured on a LCL-CBED pattern is [2]:

$$|\underline{G}| = (2\,|\underline{k}|\,|\underline{H}|)^{1/2} \qquad (1)$$

where $|\underline{k}| = \frac{1}{\lambda}$ and $|\underline{H}|$ is the HOLZ spacing along [uvw], where [uvw] is parallel (or approximately parallel) to the electron beam. Hence $|\underline{H}|$ can be determined. Now, $|\underline{H}|$ can also be calculated from:

$$|\underline{H}| = \frac{p}{|[uvw]|} \qquad (2)$$

where, for a fcc phase: p=1 if u+v+w is odd (3)

p=2 is u+v+w is even (4)

and for a b.c.c phase: p=2 if uvw are all odd (5)

p=1 otherwise (6)

and |[uvw]| is the modulus of the real space vector along, $\underline{H}$. Hence, the measured (equation (1)) and calculated (equation (2)) values of $|\underline{H}|$ can be compared and crystal structure information may be obtained routinely from single CBED patterns.

3. RESULTS

3.1 The Austenite to Proeutectoid Ferrite Reaction

Figure 1 is an SEM image of steel A which had been isothermally transformed at 575°C for 60s.* The austenite, most of which transforms to martensite during the quench, can be differentiated from the proeutectoid ferrite since:

(i) the martensite/austenite is attacked less readily than the ferrite. Hence, strong topographic contrast is obtained from the martensite/ferrite interfaces (figure 1):

(ii) the substructure within the martensite is often etched lightly so that these regions appear mottled (figure 1).

Reference to figure 1 reveals some interesting features. For example:

(iii) austenite of a very high aspect ratio is observed, e.g., at A+

(iv) the curvature of austenite island A in the vicinity of B is strongly suggestive of a "pinching-off" process, i.e., this island will split eventually to form two smaller islands. A second example of this latter process is arrowed C;

(v) the observed bowing of the ferrite grain boundary in the vicinity of austenite pool D indicates that this austenite island is exerting a Zener [3,4] drag force on the boundary and that ferrite grain growth is occurring;

(vi) austenite pool E appears to be completely embedded in the proeutectoid ferrite. This implies that ferrite grain F has enveloped this latter pool of austenite during grain growth;

(vii) a number of the austenite pools are very small. For example, pool G is only 3μm in diameter.

---

* The phenomena discussed with respect to this, and the other figures presented, are general. Hence, for subsequent micrographs, the transformation temperatures and times will be given in the figure captions only.

+ The term austenite will be employed for the remainder of the text since the focus of this paper is on the high temperature phase transformations; (i.e., austenite to ferrite and carbide) and not the austenite to martensite transformation which occurs during the quench.

Figure 2 is a further SEM image of the ferrite/austenite aggregate and shows that a series of small (~1μm), austenite pools are present, both within the ferritic matrix (A) and on ferrite grain boundaries (B). It is also of interest to note that the "intragranular" islands of austenite are approximately spherical. That the features labelled A and B on figure 2 are indeed austenite can be shown by noting that, for this specimen (Steel B; transformed for 60s at 575°C) no pearlite or cementite was present as confirmed by transmission electron microscopy (TEM). In addition, no other second phase particles of similar dimensions were ever observed. In addition, the frequency with which intragranular pools of austenite were observed rules out the possibility of these being "artifacts" due to sectioning.

Confirmation of the above was obtained using TEM. Figures 3 and 4 are examples of small pools of austenite at a ferrite grain boundary and within the ferritic matrix respectively. The presence of stacking faults in the particles shown in Figures 3a and 4a together with the associated diffraction patterns of figures 3b and 4b shows that these small pools did not transform to martensite during the quench. In figure 3a, the position of the grain boundary is indicative that the by-pass process is almost complete, and the austenite is almost completely embedded in proeutectoid ferrite grain B. The LCL-CBED pattern of figures 3b was analyzed as follows. The intersection of the 400 and 022 Kikuchi lines (arrowed A and B respectively) defined the position of the $[0\bar{1}1]_\gamma$ pole (denoted by the circle), and the position of the $[O\bar{1}\Gamma]_\lambda$ FOLZ is arrowed C. Hence $|\underline{G}|$ could be measured (5.227Å^{-1}) and $|\underline{H}|$ calculated (0.43Å^{-1}). This latter calculated value compares favorably with the theoretical value of $|\underline{H}|\,[0\bar{1}1]$ ($0.40\ \text{Å}^{-1}$). Hence, the intergranular particle (C) on figure 3 can be identified unambiguously, as austenite. Although many of the small austenite particles were retained after quenching, others transformed to martensite as is shown in Figures 5a,b. Reference to Figures 3-5 shows that the small austenite pools are either approximately spherical (Figures 2a, 4a and 5a) or are faceted (Figure 5b). Similar morphologies were documented using the SEM, i.e., faceted (at D, E and H on Figure 1) and spherical (at A Figure 2). For the small intergranular particles, facetted interfaces were

observed in association with one abutting ferrite grain (A in figure 3a). However, smoothly curved interfaces frequently were observed with respect to the second ferrite grain (B in figure 3a). The implications of these observations are deferred to the discussion section.

In contrast with many of the small pools, larger pools of austenite always transformed to martensite on quenching. This is consistent with a number of earlier studies [5-8].

3.2 The Austenite to Ferrite Plus Carbide Reactions

In this section, some representative examples of fully transformed (i.e. ferrite/carbide aggregates) structures are presented. Further details are given in Lee et. al. [1]. Figure 6 shows a relatively large (~ 30 μm in length) pearlite nodule. However, discrete particles of cementite are observed in the ferritic matrix, e.g., at A (for this transformation schedule, no retained austenite was observed). Figure 7 presents a further example of a moderately large pearlite colony in fully transformed specimen material. However, in addition to pearlite, massive films of cementite are observed on the ferrite grain boundaries (arrowed A) and at proeutectoid ferrite pearlite/interfaces (arrowed B). Finally, figure 8 shows "discrete" precipitates of cementite on a ferrite grain boundary. These precipitates are associated with "puckering" of the grain boundary.

In the following section, these observations concerning the ferrite/carbide aggregates will be discussed in relation to the results presented in Section 3.1 and new models for the decomposition of austenite will be presented.

4. DISCUSSION

4.1 Encapsulation of Austenite by Ferrite

The results presented in section 3.1 suggest that :

(i) the prior austenite grains can be partitioned by proeutectoid ferrite;

(ii) the resultant small pools of austenite exert a drag force on the migrating ferrite grain boundaries;

(iii) the ferrite grain boundaries can breakaway eventually, leading to intragranular austenite.

A possible sequence of events which will lead to the encapsulation of small pools of austenite is shown in figure 9. Initially it is assumed that shape instabilities develop at the austenite/ferrite interface (Figure 9a); a number of these shape instabilities are arrowed on Figure 11 and see Figure 1, at B. Although the origin of these shape instabilities is uncertain, they may be formed in a manner which is similar to that discussed by Shewmon [9], i.e., they are incipient Widmanstätten side plates. Enhanced diffusion of carbon away from the protrusions will then lead to "pinching off," which will yield discrete pools of austenite at the ferrite grain boundary (Figure 9b). A particularly striking example of the "pinching-off" process is given in Figure 12 where it can be seen that at least three discrete regions (A, B, C) are forming from one original pool of austenite. A further example is provided in figure 1 where particles D, E and H are faceted and each particle displays at least one mutually parallel facet. This is strong evidence that these latter particles have identical crystallographic orientations, i.e., they formed from the same prior austenite grain.

Once the ferrite grain boundary has been created (figure 9b) it is subjected to normal grain growth forces and individual boundaries will migrate towards their centers of curvature. This driving force for grain growth, will be counterbalanced by the Zener drag force. However, reference to e.g., Figures 2, 3a and 5 shows that the driving force frequently outweighs the restraining force and hence, the ferrite boundaries will move around the austenite particles and finally break free. When the boundary breaks free, the austenite particle remains embedded in the ferrite matrix. These latter two stages are shown schematically in Figures 9 c,d and in the experimental image of Figure 13 (arrowed).

However, for all aging times and temperatures investigated, many of the austenite

pools remained at the ferrite grain boundaries. This can be explained in terms of the nature of the drag force. It is assumed, to a first approximation, that the austenite pools are spherical and of radius r, then the force (F) to remove the ferrite boundary from a single pool of austenite is given by:

$$F = \pi r \gamma \qquad (7)$$

where γ is the ferrite grain boundary energy. Hence the large pools of austenite will exert a much larger retarding force and ferrite grain growth will be suppressed. Eventually, these large regions will transform to pearlite. This is exactly what happens as evidenced by the images of Figures 6 and 7.

Now, if a single, large pool of austenite of radius r_0 partitions to form N pools of austenite, each of radius r_1, then the total drag force will decrease since the total area of boundary destroyed after partitioning ($N.\pi r_1^2$) will be less than that of the single, large pool of austenite, prior to partitioning (πr_0^2). This follows since the pinching-off process, creates ferrite grain boundary area. Hence, partitioning will promote encapsulation.

Austenite islands A-C (Figure 12) formed from a single prior austenite grain by a "pinching-off" process. Due to their close proximity, it is also highly likely that pools D and E formed from the same austenite grain. This implies that a second mechanism of partitioning is operative i.e., partitioning can occur by the preferential growth of Widmanstätten side plates* (The plate-like nature of the ferrite grain F in Figure 12 substantiates this hypothesis). It should be noted that this latter mechanism would not operate at 700°C since Widmanstätten ferrite side plate. were not observed at this temperature [1].

* A good example of partitioning by Widmanstätten side plates is also shown in Figure 1 of Lee et al [1].

When the austenite became embedded in the ferrite, it adopted either an approximately spherical (Figures 2, 4a) or a faceted (Figures 1,5b) morphology. A spherical shape will result when the austenite/ferrite interfacial energy is isotopic. This in turn could be taken as evidence that many of the austenite particles are bounded by high energy incoherent interfaces. Conversely, the observation of faceting (Figures 1, 5b) implies that these latter particles are bounded, at least in part, by semicoherent interfaces. Hence, it is likely that both semi-coherent and incoherent interfaces are mobile during the decomposition of austenite in these alloys. In this context, the morphology of the austenite particle shows in figure 3a is of interest. It is suggested that low energy semi-coherent interface with respect to grain A, is being replaced by higher energy, spherical interfaces in grain B.

4.2 The Formation of Ferrite/Carbide Aggregates

As noted in the previous section, for all times and temperatures for which austenite was still present, then a significant fraction of the pools were still located on grain boundaries. Reference to figures 6 and 7 shows that the large pools invariably transformed to pearlite during extended isothermal anneals. This is reasonable in that there should be plenty of time for "cooperation" [10] to be established, after multiple nucleation events of cementite, on the austenite ferrite interface, has initiated the colony [1, 11]. For the smaller intergranular austenite pools, it is suggested that cooperation is never established and the nucleation of a single (or a small number of) cementite precipitate(s) can be sufficient to transform the entire pool of austenite. A schematic diagram of this event is presented in figure 10, which is a modification of that presented in figure 9. The major difference between the two decomposition routes is in step (C) of figure 10 where it is assumed that cementite nucleates on the ferrite/austenite triple junction. This single carbide can grow by depleting the austenite pool in carbon and consequently the remaining pool transforms epitaxially to ferrite, leaving a cementite particle on the grain boundary. This precipitate can develop into a massive film, during prolonged holding at the isothermal transformation

temperature, most probably by both coarsening and impingement with adjacent cementite precipitates. An example of a massive film of cementite that formed as described above, is given in figure 14. The two coalasced particles are labeled A and B.

Concerning the observation of intragranular cementite (figures 6 and 7), their genesis are the intragranular pools of austenite which will finally transform to expitaxial ferrite plus cementite by a mechanism which is similar to that shown in figures 10c, d.

Finally, the distribution of cementite in figure 8 requires explanation. One obvious suggestion would be that these precipitates formed by nucleation and growth at the ferrite grain boundaries and due to a residual carbon supersaturation. However, a more plausible explanation would involve the decomposition of austenite pools of a high aspect ratio. Such pools are seen in e.g., figures 1, 11 and 12. Hence it is suggested that the puckering of the ferrite boundary in figure 8 is a post transformation event i.e., it occurs after impingement of the pearlite with the adjacent proeutectoid ferrite grain.

5. CONCLUSIONS

It has been found that the growth of proeutectoid ferrite in two low carbon lamination steels partitions the austenite into a number of much smaller units. Ferrite grain growth occurs and envelopment of many of the small austenite particles occurs. The large austenite pools on ferrite grain boundaries invariably transform to pearlite. However, the small intergranular pools yield discrete carbide particles upon transformation. These discrete precipitates of cementite can develop into massive films of cementite during prolonged holding at elevated temperatures. Finally, intragranular pools of austenite yield single cementite particles together with epitaxial ferrite.

ACKNOWLEDGEMENTS

Three of the authors (J-WL, SWT and PRH) wish to acknowledge the American Iron and Steel Institute and the Atlantic Richfield Foundation for the initial financial

support. Subsequent financial support (for RV and PRH) from The Office of Naval Research-Grant No. N00014-89-J1958 is also gratefully acknowledged. SWT gratefully acknowledges support by the Advanced Steel Processing and Products Research Center at the Colorado School of Mines. The authors are also grateful to G. Ludkovsky of Inland Steel, Chicago for the supply of specimen materials.

REFERENCES

1. J-W. Lee, S.W. Thompson and P.R. Howell, J. Mat. Sci., 25 (1990) 1699.

2. J. W. Steeds in "Introduction to Analytical Electron Microscopy". eds. J. J. Hren, J. I. Goldstem and D. C. Joy. Plenum Press, New York, (1979), p. 387.

3. C. Zener, Private Communication to C.S. Smith. TMS-AIME, 175, (1949), 15.

4. T. Gladmann, Proc. Roy. Soc., A, 294, (1966), 298.

5. J. M. Rigsbee and P.J. VanderArend in "Formable HSLA and Dual-Phase Steels", ed. A.T. Davenport. TMS-AIME, Warrendale, PA, (1979), p. 56

6. B.V.N. Rao and M.S. Rashid, Metall., 16, (1983), 19.

7. F.F. Yi, K.J. Yu, I.S. Kim and S.J. Kim, Met. Trans A, 14A ,(1983), 1497

8. P-H Chang, Scripta Met, 18, (1984), 1245.

9. P.G. Shewmon. "Transformations in Metals" McGraw Hill, New York. (1969), p. 219.

10. M. Hillert, in "Decomposition of Austenite by Diffusional Processes". eds. V. F. Zackay and H. I. Aaronson. Interscience. New York, (1962), p. 197.

11. S. W. Thompson and P. R. Howell Scripta Met, 22, (1988), 1775.

Table 1

Chemical Compositions of Specimen Materials

	C	Mn	Si	P	S	Al
Steel A	0.04	0.6	0.05	0.06	0.02	<0.008
Steel B	0.04	0.7	0.22	0.09	0.02	0.21

FIGURE CAPTIONS

Figure 1. Scanning Electron Microscope (SEM) image of the ferrite/austenite microstructure that develops in steel B after 5 minutes at 625°C. Note that the majority of the austenite transforms to martensite during the quench and this yields a molted appearance. Details of the microstructures are given in the text.

Figure 2. SEM image of ferrite austenite microstructure developed in steel B after 1 minute at 575°C.

Figure 3. (a) Bright field (BF) transmission electron microscope (TEM) image of an intragranular austenite particle. Note the presence of stacking faults in the austenite (Steel B. 1 minute at 575°C). (b) Low camera length convergent beam electron diffraction pattern from the austenite particle in figure 3a. See text for analysis.

Figure 4. (a) Centered dark field (CDF) of an intragranular austenite particle (Steel B. 1 minute at 575°C). (b) Selected area diffraction pattern of the austenite in figure 4a.

Figure 5. BF images of intragranular islands of austenite which transformed to martensite during the quench. (a) Steel B. 30s at 675°C. (b) Steel B. 10s at 650°C.

Figure 6. SEM image of ferrite and pearlite. Note also the intragranular cementite particles. (Steel A. 30 minutes at 550°C).

Figure 7. SEM image of ferrite and pearlite. Massive films of cementite are observed at proeutectoid ferrite/pearlite interfaces and at ferrite/ferrite grain boundaries. (Steel A. 15 hours at 650°C).

Figure 8. SEM image of cementite precipitates at a ferrite grain boundary. (Steel B. 1 hour at 625°C).

Figure 9. A schematic illustration of the formation of intragranular pools of austenite.

(a) Formation of shape instabilities at the austenite/ferrite interface which leads to;

(b) pinching-off of the austenite into discrete pools at ferrite grain boundaries.

(c) Migration of the ferrite grain boundary around the austenite. The driving force is that for normal grain growth, leading to;

(d) complete encapsulation of the austenite pool in the ferritic matrix (α_1).

Figure 10. A schematic illustration of the formation of intergranular cementite.

(a) and (b) As for figure 9.

(c) Nucleation of cementite at the $\gamma / \alpha_1 / \alpha_2$ triple junction.

(d) Formation of grain boundary cementite by epitaxial growth of α_1 and α_2 into the carbon depleted austenite.

Figure 11. SEM image of many, small pools of austenite. For discussion: see text. (Steel B. 1 minute at 575°C).

Figure 12. SEM image of the pinching-off process (Steel A. 1 minute at 550°C).

Figure 13. SEM image of the various stages of encapsulation (Steel B. 1 minute at 550°C).

Figure 14. TEM image of a massive film of cementite at a ferrite grain boundary (Steel A. Slowly cooled from the austenite range to room temperature).

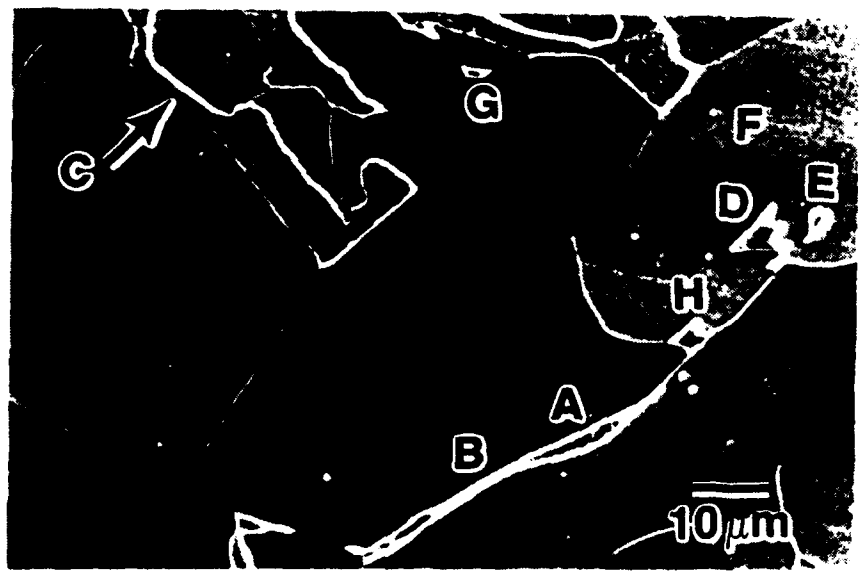

1

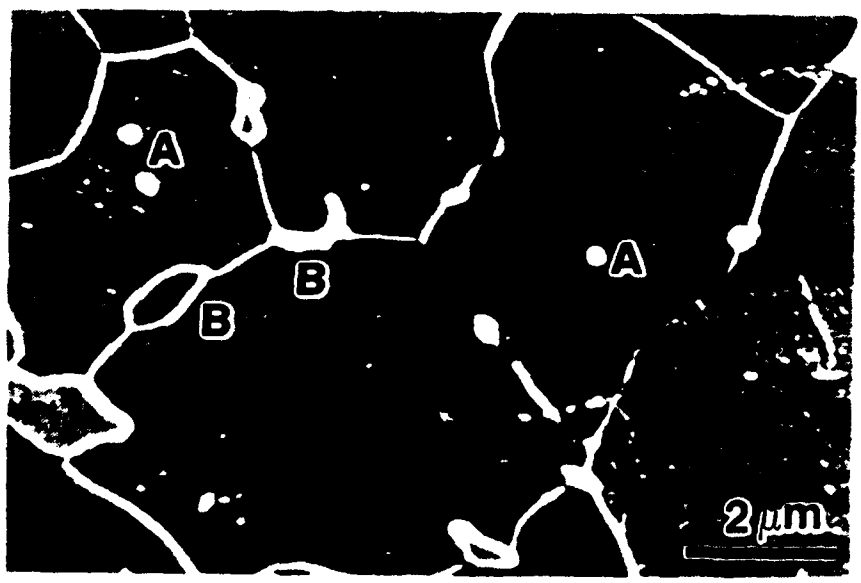

2

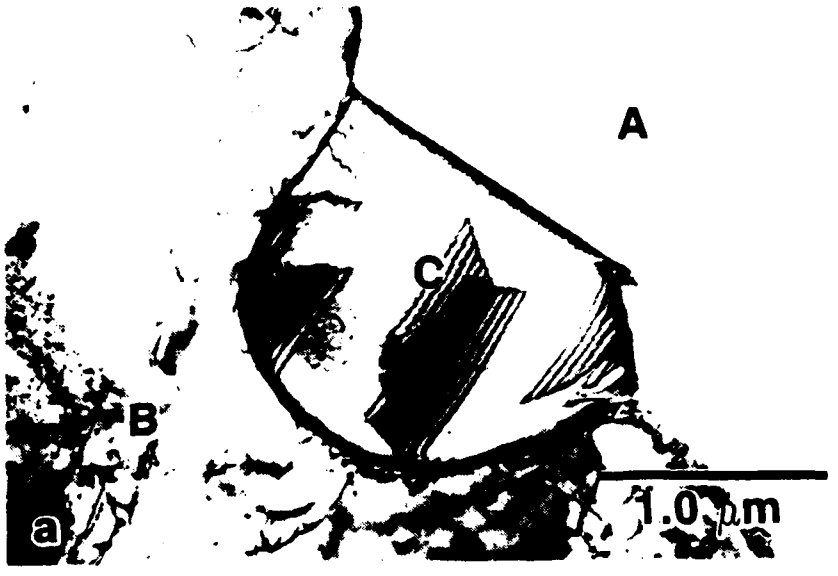

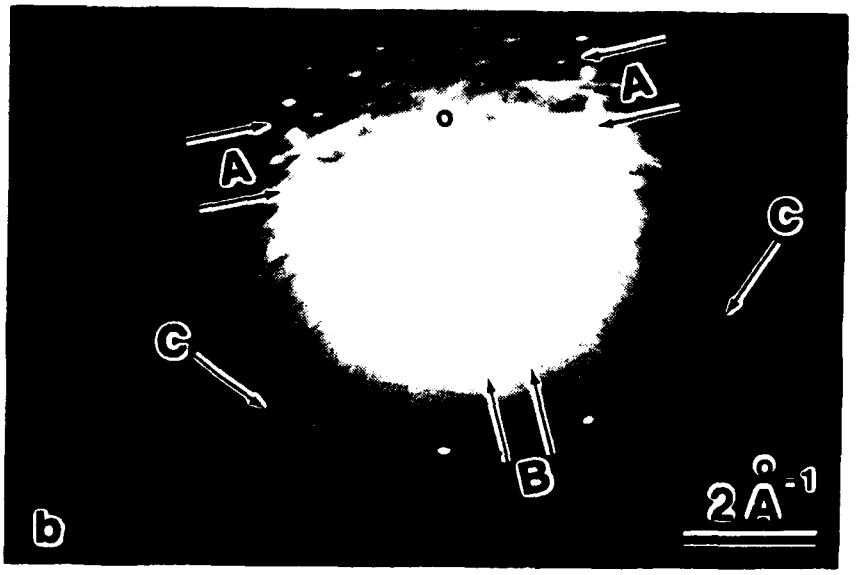

3

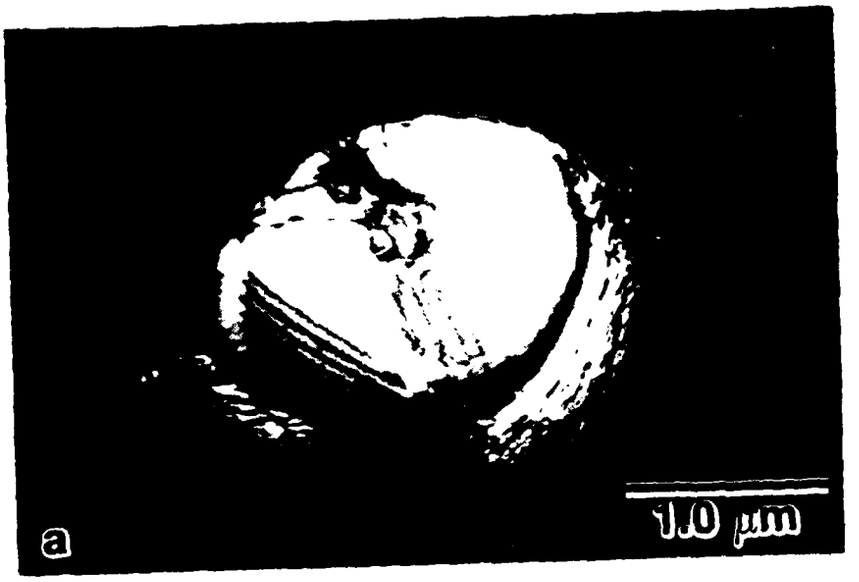

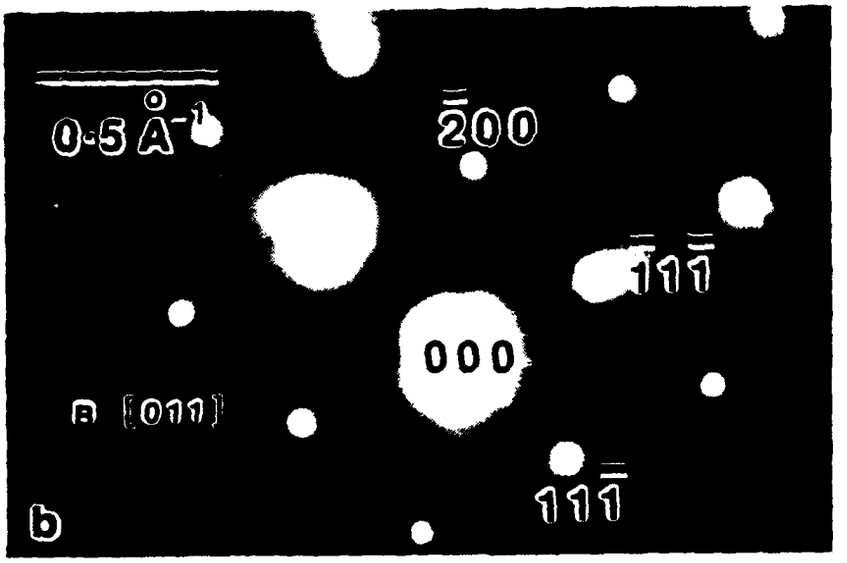

4

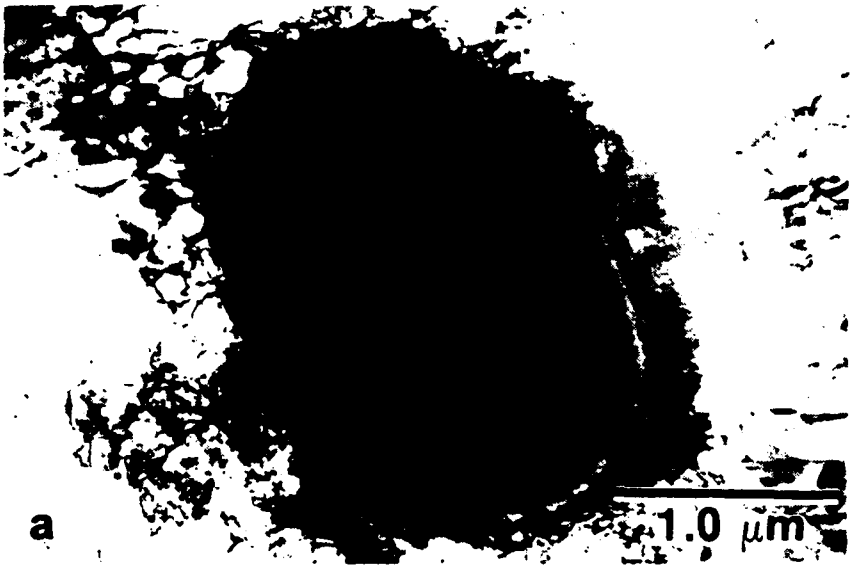

5

6

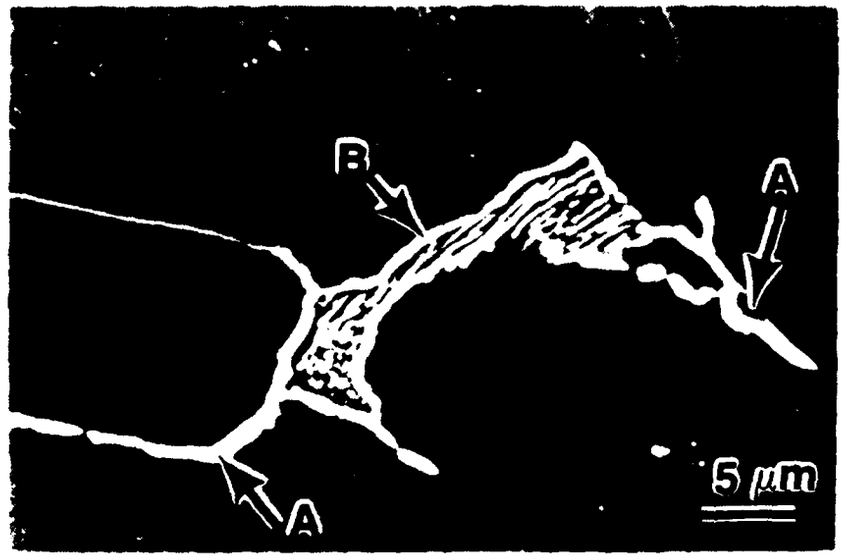

7

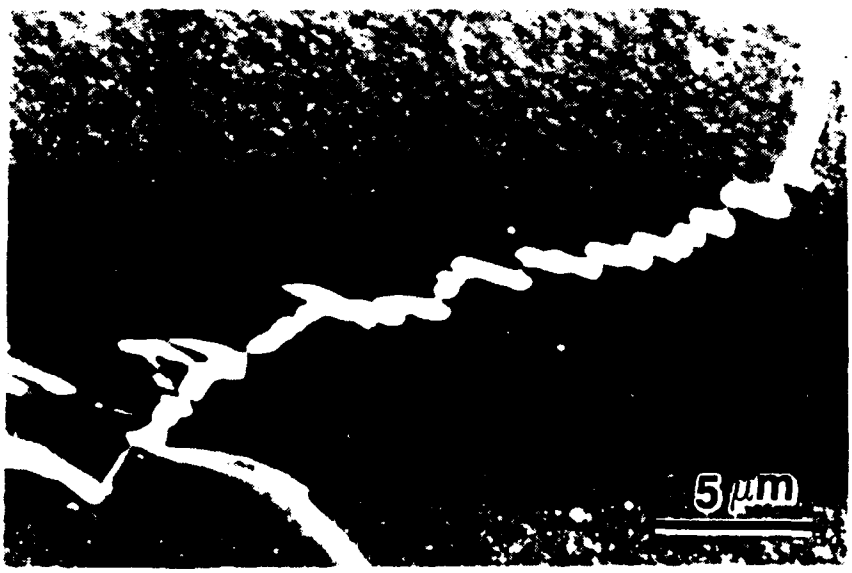

8

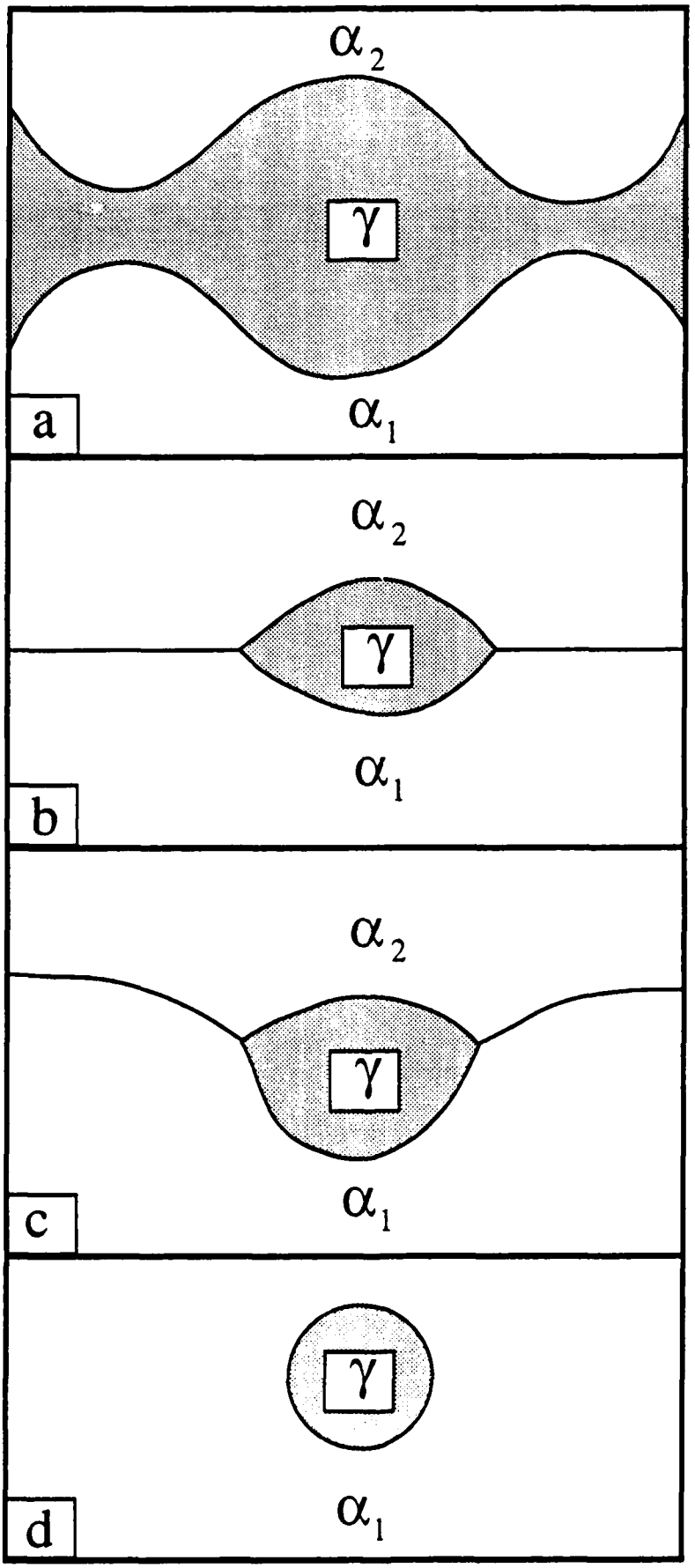

9

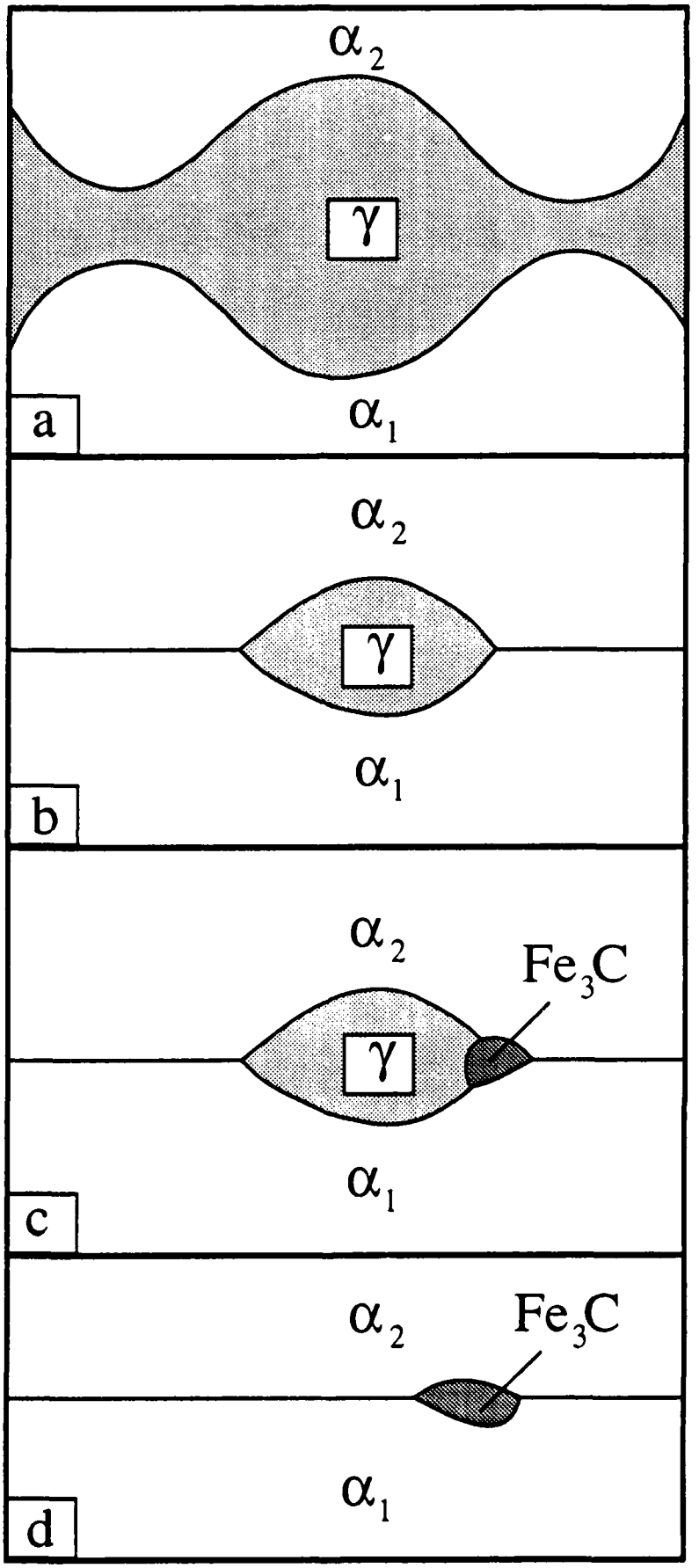

10

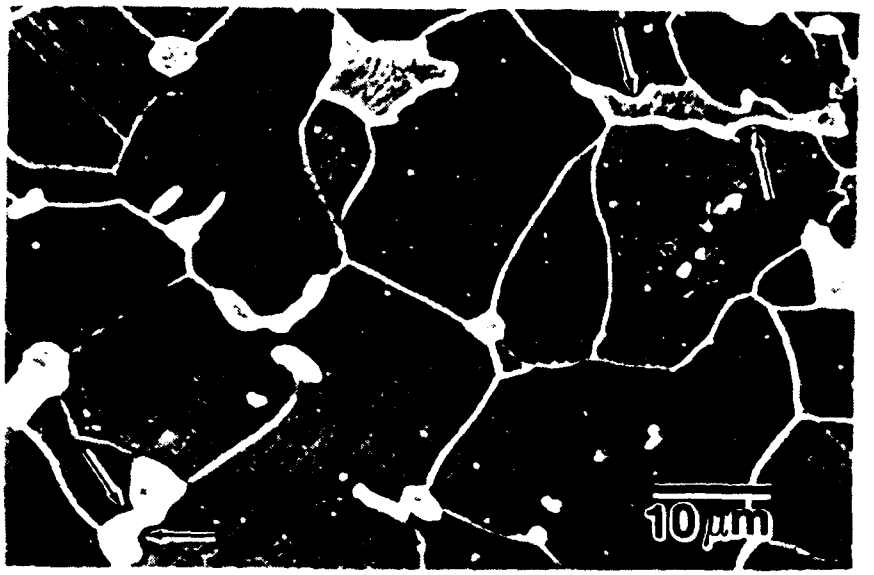

11

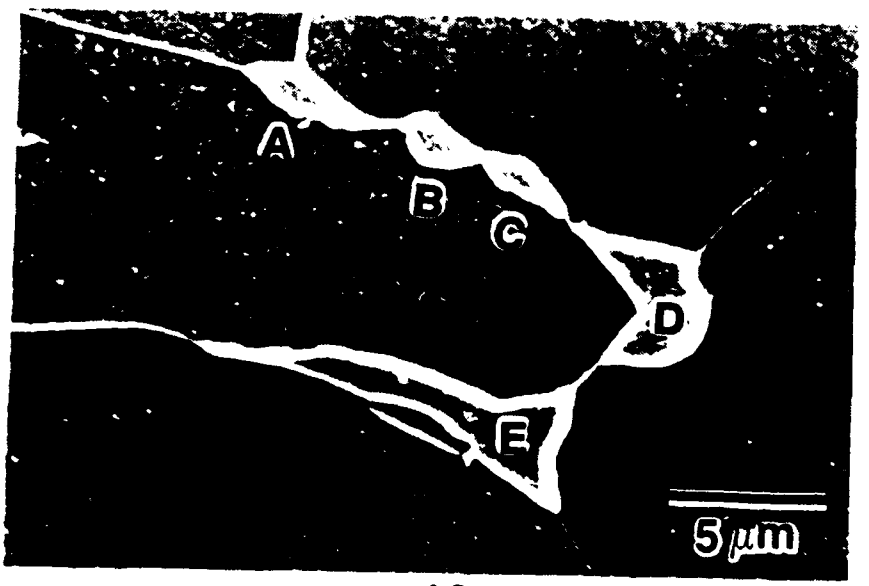

12

13

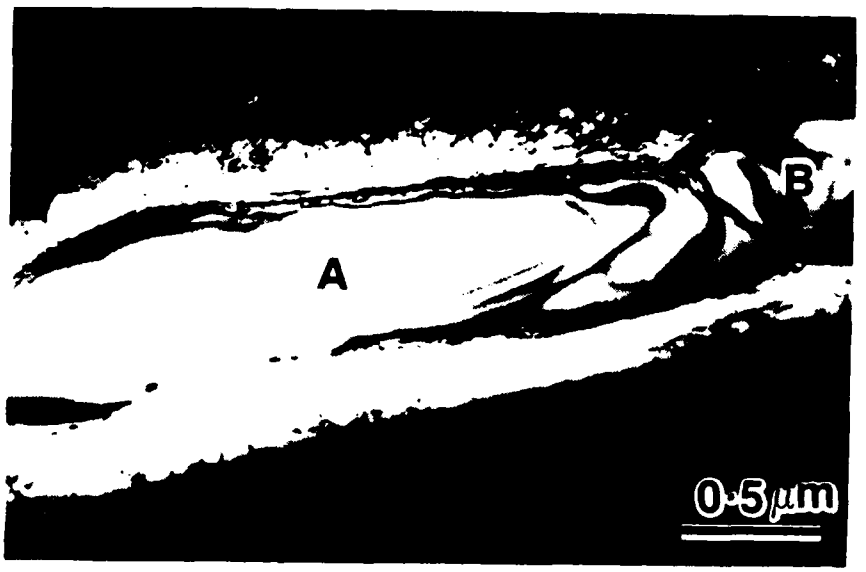

14

G. W. Bailey, Editor, Proceedings of the 49th Annual Meeting of the Electron Microscopy Society of America

To be published in : " *Proc 49th Annual Meeting of EMSA* "
ed. G.W. Bailey. EMSA, San Francisco, CA

TITLE ➡ # GRANULAR BAINITE OR GRANULAR FERRITE ?- A PRELIMINARY TEM INVESTIGATION OF AN HSLA-100 STEEL

R. Varughese,* S. W. Thompson,** and P. R. Howell*

* Dept. of Materials Science and Eng., The Pennsylvania State University, University Park, PA 16802
** Advanced Steel Processing and Products Research Center, Dept. of Metallurgical and Materials Eng., Colorado School of Mines, Golden, CO 80401

Ever since Habraken and Economopoulos[1] first employed the term *granular bainite* to classify certain unconventional transformation products in continuously cooled steels, the term has been widely accepted and used, despite the lack of a clear consensus as to the detailed nature of the transformation products which constitute *granular bainite*. This paper presents the preliminary results of a TEM investigation of an 0.04 wt% C, copper-containing steel (designated HSLA-100). It is suggested that the term *granular ferrite*[2] rather than *granular bainite* is a more accurate description of this multiphase reaction product.

Figure 1 is a light micrograph of a sample which had been air-cooled from 900°C to room temperature. The microstructure is typical of that which has been termed *granular bainite* in the past and appears to consist of equiaxed ferritic grains together with other *minor transformation products*. In order to examine these structures in more detail, both continuously cooled and isothermally transformed and quenched materials have been examined with TEM. *Granular bainite* has been found in virtually all samples. Figure 2 is a combined austenite/ ε-copper centered dark field(CDF) image of a sample which had been slowly cooled and subsequently tempered to yield the dispersion of ε- Cu. Small pools of retained austenite (arrowed) are present, both at the ferrite grain boundaries and intragranularly. The fact that all of the austenite islands in this region are illuminated in this CDF indicates strongly that, prior to transformation, they all belonged to the same grain of austenite. In many instances, the austenite pools transformed to martensite, and an example is given in the bright field(BF)/CDF pair of figures 3a,b from the air-cooled sample. In this instance, both pools of martensite are contained within the same equiaxed grain of ferrite, and the CDF image of figure 3b indicates that again, these two regions of martensite originated from the same austenite grain. Finallv, figures 4 a,b are a BF/ martensite CDF pair from a sample which had been transformed for 30 minutes at 450 °C. Several intergranular pools of martensite and one intragranular pool of martensite are marked M.

Reference to figures 2-4 shows that *granular bainite* is a microconstituent comprising equiaxed ferrite (the dominant phase) together with a dispersion of austenite/ martensite pools. This observation is broadly consistent with a recently published report on a similar steel[2]. Hence it is considered that this multiphase product should not be termed *bainite* in that it is not consistent with either of the current definitions of bainite in steels, which are in essence: (i) the noncooperative growth of ferrite and cementite[3], and (ii) the coupled diffusional/ displacive growth of ferrite plates / laths[4]. No cementite has been observed and the ferrite is equiaxed. Hence, the term *granular ferrite* is considered to be more apropos.

References

1. L. J. Habraken and M. Economopoulos, in Transformation and Hardenability in Steels, Climax Molybdenum Company, Michigan (1967) 69.
2. S.W. Thompson et al., Metall. Trans., 21A (1990) 1493.
3. H. I. Aaronson et al., Metall. Trans., 21A (1990) 1343.
4. G. B. Olson et al., Metall. Trans., 21A (1990) 805.
5. Two of the authors (RV and PRH) gratefully acknowledge the support of The Office of Naval Research - Grant No. N00014-89-J1958. SWT gratefully acknowledges support by the Advanced Steel Processing and Products Research Center at the Colorado School of Mines.

FIG.1.--Light micrograph of air-cooled sample.

FIG.2.--Austenite/ ε-Cu centered dark field (CDF) image.

FIG.3.--Air-cooled material: (a) BF image of equiaxed ferrite grain containing discrete pools of martensite (marked M). (b) Corresponding martensite CDF image.

FIG.4.--(a) BF image of equiaxed/ granular ferrite with intergranular and intragranular martensitic pools. Isothermally transformed for 30 minutes at 450 °C. (b) Corresponding martensite CDF image.